Physics of Fluids ARTICLE scitation.org/journal/phf

A lattice Boltzmann method for single- and two-phase models of nanofluids: Newtonian and non-Newtonian nanofluids

Cite as: Phys. Fluids 33, 102008 (2021); doi: 10.1063/5.0067744
Submitted: 19 August 2021 · Accepted: 1 October 2021 ·
Published Online: 21 October 2021

Gholamreza Kefayati[1,a)] and Andrew P. Bassom[2]

AFFILIATIONS

[1]School of Engineering, University of Tasmania, Hobart 7001, Tasmania, Australia
[2]School of Natural Sciences, University of Tasmania, Hobart 7001, Tasmania, Australia

Note: This paper is part of the Special Issue on the Lattice Boltzmann Method.
[a)]**Author to whom correspondence should be addressed:** gholamreza.kefayati@utas.edu.au

ABSTRACT

Nanofluids play an important role in many different industries for an improvement of heat transfer. The modeling and simulation of such fluids is developing continuously. Two important models for studying nanofluids are mixture (or single-phase) and two-phase (or Buongiorno) forms, which have been examined in various ways. Non-Newtonian behavior of nanofluids (shear-thinning and viscoplasticity) has been observed in experimental tests and simulated in several studies. However, a lattice Boltzmann method (LBM), which can employ either model depending on the particular non-Newtonian constitutive equation, has not been considered to date within the suite of available numerical methods. Here, we propose a comprehensive LBM to simulate both Newtonian and non-Newtonian nanofluids. The approach has the potential to incorporate any format of extra tensor directly and is independent to the relaxation time; the upshot is that our method is appropriate for studying non-Newtonian nanofluids. The derivations for both models are presented and discussed in some detail. To evaluate the proposed method, it was compared with previous studies into a benchmark problem, natural convection in a square enclosure filled with Newtonian nanofluids and non-Newtonian fluids. Then, the applied macroscopic and LBM equations, using the power-law and viscoplastic models, for the benchmark are derived and the results are presented.

I. INTRODUCTION

In the 1990s, Choi and Eastmann[1] introduced nanofluids as engineered colloids, which consist of a base fluid (or carrier fluid) and a small volumetric fraction of nanoparticles. The nanoparticles had a considerable effect on the thermal conductivity of the carrier fluid, which makes nanofluids a viable mechanism for improving the heat transfer in many different applications.[2–6] Two major classes of methodology have been employed in the previous studies of nanofluids. The first method is known as the single-phase (or mixture) model, which is easy to analyze and is efficient computationally since it allows us to idealize the solid/fluid mixtures as a single fluid with specific thermophysical parameters. In addition, it was concluded that this method is practicable if the focus is on the heat transfer.[7] This approach has been imposed widely in various problems and geometries by employing a suite of numerical methods in computational fluid dynamics (CFD).[7–12]

The single-phase model of nanofluids was developed for non-Newtonian power-law[13–15] and viscoplastic[16–18] fluids in limited studies, while it has been observed by many researchers in which nanofluids demonstrate non-Newtonian behavior in specific volume fractions, nanoparticles, and configurations.[4] The single-phase model makes many assumptions including ignoring Brownian motion and omitting the thermophoresis term. Although these simplifications can affect the estimated heat transfer significantly, the single-phase configuration has been adopted for many nanofluid problems owing to its straightforward and simple implementation in various numerical approaches coupled to good computational efficiency.

In the mixture model, the thermophysical properties of nanofluids are considered as functions of the nanoparticle volume fraction. The modeling of the thermal characteristics has been refined and improved with the advent of a growing album of experimental results.[1–6] The first comprehensive two-phase model of nanofluids, which have been used widely, was proposed by Buongiorno.[19] In the study, aimed at considering the relative velocities of the carrier fluid and the nanoparticles, seven different terms were evaluated. It was

found that only two of these, Brownian diffusion and thermophoresis, play the key role in nanofluids. Buongiorno's model was developed for studying the natural convection with adding an external force in the form of the gravity by Tzou[20,21] and Corcione *et al.*[22] Nield and Kuznetsov[23,24] studied the classical Rayleigh–Benard problem for nanofluids based on the model of Buongiorno. They considered particles with diameters of tens or hundreds nanometers and with very small volume fractions. Haddad *et al.*[25] studied Rayleigh–Benard natural convection with the single- and two-phase models for CuO–water nanofluids. They found that Brownian and thermophoresis terms in the two-phase model generate higher heat transfer compared to the single-phase model. The Buongiorno's model was developed for studying nanofluids in porous media to investigate convection in various configurations, porous models, and geometries.[26–28] The Buongiorno's model was developed for non-Newtonian power-law[29] and viscoplastic[18] fluids in limited studies, while it has been observed by many researchers in which nanofluids demonstrate non-Newtonian behavior in specific volume fractions, nanoparticles, and configurations.[4]

The lattice Boltzmann method (LBM) is a particle distribution function method, which has been considered as a strong alternative numerical method to common macroscopic approaches, which discretizes governing equations. The algorithm of this method is parallel and can be simply programmed for complex problems and geometries. In addition, the computational time and cost is significantly lower than for macroscopic methods, which makes it attractive in various fields, especially heat and fluid flow problems.[30–39] Xuan and Yao[40] developed and introduced an LBM for simulating nanofluids by considering a series of acting forces including one which represented the Brownian motion. However, the model did not include the Thermophoresis and Brownian terms in the energy equation. In addition, the thermal conductivity and thermal diffusion were not updated for the nanofluids although they should be altered on consideration of the volume fraction and temperature. Many studies[41–52] applied a mixture method in LBM where the thermophysical properties of nanofluids are calculated and implemented in the non-dimensional parameters. Limited studies into two-phase model of nanofluids have been made,[53,54] but these types of research did not show the details and derivations of the applied LBM approach and concentrated on the results. To the best of our knowledge, there is no a comprehensive proposed model of LBM for recovering the equations of energy and nanoparticles in the form of the Buongiorno's model and the non-Newtonian behavior of nanofluid in the case of two-phase and single-phase models.

The main objective of this study is to introduce an LBM for recovering the equations of the single-phase and two-phase models of nanofluids with developing the previous macroscopic models to non-Newtonian nanofluids.

II. THE MACROSCOPIC EQUATIONS

A. Single-phase model

The momentum and energy equations of the incompressible flow ($\nabla \cdot \mathbf{u} = 0$) of the single-phase model in the absence of the chemical reactions, radiation, heat source, and the viscous dissipation for the natural convection were given by[7–9]

$$\rho_n \frac{D\mathbf{u}}{Dt} + \nabla p - \nabla \cdot \boldsymbol{\tau} = \mathbf{f}, \tag{1}$$

$$(\rho c)_n \frac{DT}{Dt} + \nabla \cdot \mathbf{q}_c = 0, \tag{2}$$

where $\frac{D}{Dt} = \frac{\partial}{\partial t} + \mathbf{u} \cdot \nabla$, and the quantities $\rho, \mathbf{u}, t, \boldsymbol{\tau}, p, T, c$ denote the density, velocity, time, extra stress tensor, pressure, temperature, and specific heat, respectively. The subscripts *f*, *p*, and *n* refer to the fluid, nanoparticle, and nanofluid, respectively. The heat flux ($\mathbf{q}_c$) was defined by the Fourier's law of conduction ($\mathbf{q}_c = -k_n \nabla T$), where k_n is the thermal conductivity of nanofluid (or the effective thermal conductivity). In Refs. 7–9 and subsequent studies, the nanofluid was assumed to be Newtonian, so the extra tensor was calculated using $\boldsymbol{\tau} = \mu_n \mathbf{A}$, where μ_n is the nanofluid viscosity (or the effective viscosity), and $\mathbf{A}$ is the first Rivlin–Ericksen tensor ($\mathbf{A} = \nabla \mathbf{u} + \nabla \mathbf{u}^T$). In Refs. 7–9, the nanofluid viscosity was found using the Brinkman's model as $\mu_n = \frac{\mu_f}{(1-\phi)^{2.5}}$. In the mentioned studies, the nanofluid specific heat is defined by $c_n = \frac{\phi \rho_p c_p + (1-\phi)\rho_f c_f}{\rho_n}$ and the nanofluid density was given by $\rho_n = \phi \rho_p + (1-\phi)\rho_f$. The Maxwell–Garnett approximation for spherical particles was implemented for the effective (nanofluid) thermal conductivity by $\frac{k_n}{k_f} = \frac{k_p + 2k_f - 2\phi(k_f - k_p)}{k_p + 2k_f + \phi(k_f - k_p)}$. $\mathbf{f}$ is the force per volume, which was calculated for the case of natural convection by the Boussinesq approximation as $\mathbf{f} = (\rho\beta)_n \mathbf{g}(T_r - T)$, where $(\rho\beta)_n = [\phi \rho_p \beta_p + (1-\phi)\rho_f \beta_f]$. T_r and β are the reference temperature and the coefficient of thermal expansion, respectively. In the non-Newtonian nanofluids, the viscosity is written in a specific format of the shear rate ($\dot{\gamma}$), which is defined by $\dot{\gamma} = \sqrt{\frac{1}{2}\mathbf{A} : \mathbf{A}}$. It should be noted that the variables in the relation of the viscosity and shear rate can be obtained based on important effective parameters such as the nanoparticle size, temperature, and the volume fraction of nanoparticles.

B. Two-phase model

Buongiorno[19] proposed four governing equations of the two-phase model for the incompressible flow in the absence of the chemical reactions, the external forces, radiation, and the viscous dissipation as follows:

$$\nabla \cdot \mathbf{u} = 0, \tag{3}$$

$$\rho_n \frac{D\mathbf{u}}{Dt} + \nabla p - \nabla \cdot \boldsymbol{\tau} = 0, \tag{4}$$

$$(\rho c)_n \frac{DT}{Dt} + \nabla \cdot \mathbf{q} - h_p \nabla \cdot \mathbf{j} = 0, \tag{5}$$

$$\rho_p \frac{D\phi}{Dt} + \nabla \cdot \mathbf{j} = 0. \tag{6}$$

Here, $\mathbf{q}$ is the total heat flux, which is the sum ($\mathbf{q} = \mathbf{q}_c + \mathbf{q}_d$) of the conduction ($\mathbf{q}_c = -k_n \nabla T$) and the nanoparticle diffusion ($\mathbf{q}_d = h_p \mathbf{j}$). Furthermore, h is the specific enthalpy defined by $h = c\,T$. In Ref. 19, the form of thermal conductivity (k) for different nanoparticles was calculated by $k_n = k_f(1 + A\phi + B\phi^2)$, where A and B are constants. The diffusion mass flux of the nanoparticles ($\mathbf{j} = \mathbf{j}_B + \mathbf{j}_T$) is the sum of Brownian diffusion ($\mathbf{j}_B$) and Thermophoresis ($\mathbf{j}_T$) given by $\mathbf{j}_B = -\rho_p D_B \nabla \phi$, and $\mathbf{j}_T = -\rho_p D_T \frac{\nabla T}{T}$. The Brownian diffusion coefficient is defined by $D_B = \frac{k_B T}{3\pi \mu_f d_p}$, where k_B, d_p, and μ_f are the Boltzmann constant, nanoparticle diameter, and fluid viscosity,

respectively. The thermal diffusion coefficient (D_T) is given by $D_T = \varpi \frac{\mu_f}{\rho_f}\phi$, where the proportionality factor (ϖ) is defined by $\varpi = 0.26\,\frac{k_f}{2k_f+k_p}$. In Ref. 19, the nanofluid was also assumed to be Newtonian and the mixture was assumed to be dilute, which is achieved by the condition of $\phi \lll 1$, and it is valid for most cases of nanofluids ($\phi < 0.05$). Buongiorno's model was developed for studying the natural convection with adding an external force in the form of the gravity by Tzou[20,21] and Corcione *et al.*[22] Consequently, the momentum equation was modified as

$$\rho_n \frac{D\mathbf{u}}{Dt} = -\nabla p + \mu_n \nabla^2 \mathbf{u} + \mathbf{f}. \tag{7}$$

III. THE MESOSCOPIC NUMERICAL METHOD

A. The LBM for the momentum equation

The momentum equation for both single- and two-phase models of nanofluids is the same in the form of Eq. (1). The LBM equation for recovering the momentum equation can be defined as

$$\frac{\partial f_\alpha}{\partial t} + \mathbf{e}_\alpha \cdot \nabla_{\mathbf{x}} f_\alpha - F_\alpha = -\frac{1}{\varepsilon\,\lambda_f}(f_\alpha - f_\alpha^{eq}), \tag{8}$$

where f_α is the particle distribution function in the α direction, $\mathbf{e}$ is velocity at position $\mathbf{x}$, and time t for particles. The parameter ε is a small parameter, and λ_f is the non-dimensional relaxation time. The index of α represents different lattice vectors. In this method, it is possible different lattices with the definition of DmQn, where m and n represent the dimension and the number of particles. For example of two-dimensional case, the D2Q9 model and the velocity vectors are presented as Fig. 1 and will be implemented in this study. Here, σ is a constant, which is selected with considering the numerical stability and satisfying the Courant–Friedrichs–Lewy (CFL) condition (Appendix A). The equilibrium particle distribution function f_α^{eq} is found as[55–58]

$$f_\alpha^{eq} = A_\alpha + \mathbf{e}_\alpha \cdot \Gamma_\alpha + (\mathbf{e}_\alpha \otimes \mathbf{e}_\alpha) : \Lambda_\alpha, \tag{9}$$

where A_α, Γ_α, and Λ_α are a constant, a vector, and a matrix, respectively. The parameters in the D2Q9 are found as

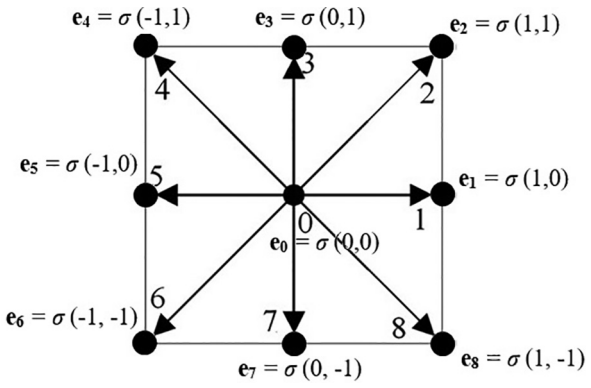

FIG. 1. Discrete velocity distribution in D2Q9.

$$A_0 = \rho_n - \frac{2p}{\sigma^2} - \frac{\rho_n |\mathbf{u}|^2}{\sigma^2}, \quad A_\alpha = 0, \quad \alpha = 1, \ldots, 8 \tag{10}$$

and

$$\Gamma_\alpha = \frac{\rho_n \mathbf{u}}{2\sigma^2}, \quad \alpha = 1,3,5,7; \quad \Gamma_\alpha = \mathbf{0}, \quad \alpha = 2,4,6,8. \tag{11}$$

Next,

$$\Lambda_\alpha = \begin{bmatrix} \Lambda_{11} & 0 \\ 0 & \Lambda_{22} \end{bmatrix}, \quad \alpha = 1,3,5,7, \tag{12}$$

$$\Lambda_{11} = \frac{1}{2\sigma^4}(p + \rho_n u^2 - \tau_{xx}), \quad \Lambda_{22} = \frac{1}{2\sigma^4}(p + \rho_n v^2 - \tau_{yy}), \tag{13}$$

and

$$\Lambda_\alpha = \begin{bmatrix} 0 & \Lambda_{12} \\ \Lambda_{21} & 0 \end{bmatrix}, \quad \alpha = 2,4,6,8, \tag{14}$$

$$\Lambda_{12} = \Lambda_{21} = \frac{1}{8\sigma^4}(\rho_n uv - \tau_{xy}). \tag{15}$$

u and v are velocities in x and y directions. p is the pressure, and τ_{xx}, τ_{yy}, $\tau_{yx} = \tau_{xy}$ are the stresses. The force term F_α in (8) can be defined as

$$F_\alpha = \frac{1}{2\sigma^2}\begin{cases} \mathbf{0}, & \alpha = 0,2,4,6,8, \\ \mathbf{f}\cdot\mathbf{e}_\alpha, & \alpha = 1,3,5,7. \end{cases} \tag{16}$$

The derivations and proves for recovering the momentum equation are provided in Appendix B.

B. The LBM for recovering the energy equation

In contrast with the momentum equation, the energy equation in the single- and two-phase models is different. In fact, the single-phase model is the simplified format of the two-phase model in the absence of the diffusion mass flux of nanoparticles ($\mathbf{j} = 0$), so first the two-phase model is discussed and then substitutes the relation of $\mathbf{j} = 0$ in the equations to find the single-phase relations.

1. Two-phase model

For the energy equation, an energy distribution function g_α is introduced as

$$\frac{\partial g_\alpha}{\partial t} + \mathbf{e}_\alpha \cdot \nabla_{\mathbf{x}} g_\alpha - G_\alpha = -\frac{1}{\varepsilon\lambda_g}(g_\alpha - g_\alpha^{eq}). \tag{17}$$

λ_g is the relaxation time in the collision part of the energy distribution function. The equilibrium energy distribution function g_α^{eq} has the following linear form as

$$g_\alpha^{eq} = D_\alpha + \mathbf{e}_\alpha \cdot \mathbf{E}_\alpha, \tag{18}$$

where the scalar parameter D_α is defined such that

$$D_\alpha = (\rho c)_n T, \quad \alpha = 0; \quad D_\alpha = 0, \quad \alpha = 1, \ldots, 8. \tag{19}$$

The vectors $\mathbf{E}_\alpha$ are expressed as

$$\mathbf{E}_\alpha = \frac{1}{2\sigma^2}\left[(\rho c)_n \mathbf{u} T + \mathbf{q}\right], \quad \alpha = 1,3,5,7, \tag{20}$$

$$\mathbf{E}_\alpha = \mathbf{0}\,, \quad \alpha = 0, 2, 4, 6, 8. \tag{21}$$

Finally, the parameter G_α is obtained as

$$G_\alpha = -h_p \nabla \cdot \mathbf{j}, \quad \alpha = 1, 3, 5, 7, \tag{22}$$

$$G_\alpha = 0, \quad \alpha = 0, 2, 4, 6, 8. \tag{23}$$

2. Single-phase model

In the single-phase model, the only difference is observed in the parameters of g_α^{eq} as

$$D_\alpha = (\rho c)_n T, \quad \alpha = 0\,; \quad D_\alpha = 0, \quad \alpha = 1, \ldots, 8. \tag{24}$$

The vectors $\mathbf{E}_\alpha$ are revised as

$$\mathbf{E}_\alpha = \frac{1}{2\sigma^2}\left[(\rho c)_n \mathbf{u} T + \mathbf{q}_c\right], \quad \alpha = 1, 3, 5, 7, \tag{25}$$

$$\mathbf{E}_\alpha = \mathbf{0}\,, \quad \alpha = 0, 2, 4, 6, 8, \tag{26}$$

and

$$G_\alpha = 0, \quad \alpha = 0, \ldots, 8. \tag{27}$$

The derivations and proves for recovering the energy equation are provided in Appendix C.

C. The LBM for recovering the nanoparticle equation in the two-phase model

For the nanoparticles, a new distribution function s_α is employed as

$$\frac{\partial s_\alpha}{\partial t} + \mathbf{e}_\alpha \cdot \nabla_{\mathbf{x}} s_\alpha = -\frac{1}{\varepsilon \lambda_s}(s_\alpha - s_\alpha^{eq}). \tag{28}$$

The introduced equilibrium nanoparticle distribution function s_α^{eq} is defined as

$$s_\alpha^{eq} = \Pi_\alpha + \mathbf{e}_\alpha \cdot \mathbf{\Omega}_\alpha, \tag{29}$$

where

$$\Pi_\alpha = \begin{cases} \rho_p\, \phi, & \alpha = 0, \\ \mathbf{0}, & \alpha = 1, \ldots, 8 \end{cases} \tag{30}$$

and

$$\mathbf{\Omega}_\alpha = \begin{cases} \dfrac{1}{2\sigma^2}\left[\rho_p\, \mathbf{u}\phi + \mathbf{j}\right], & \alpha = 1, 3, 5, 7, \\ \mathbf{0}, & \alpha = 2, 4, 6, 8. \end{cases} \tag{31}$$

The derivations and proves for recovering the nanoparticle equation are provided in Appendix D.

D. Algorithm

The splitting method is used to solve the distribution function equations (8), (17), and (28). Hence, the equations are broken into two parts. The first parts of the equations are called *streaming* and are defined as

$$\frac{\partial f_\alpha}{\partial t} + \mathbf{e}_\alpha \cdot \nabla_{\mathbf{x}} f_\alpha - F_\alpha = 0, \tag{32}$$

$$\frac{\partial g_\alpha}{\partial t} + \mathbf{e}_\alpha \cdot \nabla_{\mathbf{x}} g_\alpha - G_\alpha = 0\,, \tag{33}$$

$$\frac{\partial s_\alpha}{\partial t} + \mathbf{e}_\alpha \cdot \nabla_{\mathbf{x}} s_\alpha = 0\,. \tag{34}$$

Equations (32)–(34) are solved by the finite difference method of Lax and Wendroff.[59] The second parts of the functions, which are obtained from the splitting method, are called *collision*, which are found as

$$\frac{\partial f_\alpha}{\partial t} = -\frac{1}{\varepsilon \lambda_f}(f_\alpha(\mathbf{x}, t) - f_\alpha^{eq}(\mathbf{x}, t)), \tag{35}$$

$$\frac{\partial g_\alpha}{\partial t} = -\frac{1}{\varepsilon \lambda_g}(g_\alpha(\mathbf{x}, t) - g_\alpha^{eq}(\mathbf{x}, t)), \tag{36}$$

$$\frac{\partial s_\alpha}{\partial t} = -\frac{1}{\varepsilon \lambda_s}(s_\alpha(\mathbf{x}, t) - s_\alpha^{eq}(\mathbf{x}, t)). \tag{37}$$

To solve the above collision equations, $\varepsilon\lambda = \Delta t$ and Euler method is used, so the equations are changed to

$$f_\alpha(\mathbf{x}, t^*) = f_\alpha^{eq}(\mathbf{x}, t), \tag{38}$$

$$g_\alpha(\mathbf{x}, t^*) = g_\alpha^{eq}(\mathbf{x}, t), \tag{39}$$

$$s_\alpha(\mathbf{x}, t^*) = s_\alpha^{eq}(\mathbf{x}, t), \tag{40}$$

where $t^* = t + \Delta t$. The numerical processes are as follows:

- The boundaries and initial conditions provide us with the first macroscopic values of $(\mathbf{u}, p, T, \phi)$, and then, the initial amounts of f_α^{eq}, g_α^{eq}, and s_α^{eq} are calculated using (9), (18), and (29), respectively. This section of the algorithm is considered as the zero time.
- The initial values of f_α, g_α, and s_α at time t is calculated by the collision part. In fact, they are equal to the equilibrium distribution functions.
- With f_α, g_α, and s_α at time t, the next values of the parameters are calculated by solving the streaming equations of (32), (33), and (34).
- Using the new calculated f_α, g_α, and s_α, the updated macroscopic parameters $(\mathbf{u}, p, T, \phi)$ for all grids and boundary conditions are calculated.
- With the new obtained macroscopic quantities over the domain, the corresponding f_α^{eq}, g_α^{eq}, and s_α^{eq} are renewed in (9), (18), and (29).
- In the collision part, the next time values of f_α, g_α, and s_α, using (38), (39), and (40) are calculated.
- The mentioned steps are repeated to satisfy the convergence criteria as

$$\left|\rho_n - \sum_{i=0}^{8} f_i(\mathbf{x}, t)\right| < \delta\,, \quad \left|\sqrt{|\mathbf{u}^{n+1}| - |\mathbf{u}^n|}\right| \le \delta\,, \quad \left|\sqrt{T^{n+1} - T^n}\right| \le \delta\,, \quad \left|\sqrt{\phi^{n+1} - \phi^n}\right| \le \delta\,, \tag{41}$$

where $\delta = \Delta t^2$.

E. Boundary conditions

In common LBM, different complex equations for each distribution functions of f, g, s are applied in any specific boundary conditions. Yet,

in the present study, there is the opportunity to impose various boundary conditions directly, using the macroscopic variables similar to macroscopic numerical methods. In fact, any format of Neumann and the Dirichlet boundary conditions of macroscopic parameters ($\mathbf{u}$, T, p, ϕ) provide the relations or values on the boundaries, which are used for calculating f_α^{eq}, g_α^{eq}, and s_α^{eq} using Eqs. (9), (18), and (29). Then, the f_α, g_α, and s_α are obtained through the collision part simply, following Eqs. (38), (39), and (40). The obtained values of f_α, g_α, and s_α on the boundaries are implemented for finding the interior values of f_α, g_α, and s_α in the studied grid, using the streaming equations of (32)–(34), so it demonstrates that we do not need any extra distribution functions for boundaries and the macroscopic boundaries just need to be written in the code straightforwardly. It is discussed in detail in Refs. 55–58.

IV. VALIDATION AND NUMERICAL EXAMPLES

A. Power-law model

1. Single-phase model

First, natural convection of nanofluid, which shows power-law fluid behavior in a two-dimensional cavity with the length of L, is investigated (see Fig. 2). The left and right vertical walls have high (T_H) and low (T_C) temperatures, while the horizontal walls are adiabatic. In addition, velocity is zero in all boundary conditions in the enclosure. For the problem, the dimensional momentum and energy equations of the single phase are (1) and (2), respectively. The force term ($\mathbf{f}$) is the buoyancy term, which follows the Boussinesq approximation. The extra stress tensor of the power-law non-Newtonian fluid is defined by $\boldsymbol{\tau} = K\,\dot{\gamma}^{(m-1)}\,\mathbf{A}$, following the Ostwald–de Waele model, where $\dot{\gamma}$, K, and m are the shear rate, the consistency factor, and the power-law index, respectively, which can be dependent to the volume fraction, temperature, and the diameter of particles (ϕ, T, d).[60–65] The following ratio and non-dimensional parameters are imposed:

$$\bar{\rho} = \frac{\rho_n}{\rho_f}, \quad \bar{c} = \frac{c_n}{c_f}, \quad \bar{k} = \frac{k_n}{k_f}, \quad \bar{\beta} = \frac{\beta_n}{\beta_f}, \tag{42a}$$

$$U = \sqrt{g\beta_n \Delta T L}, \quad \mathbf{u}' = \frac{\mathbf{u}}{U}, \quad \mathbf{x}' = \frac{\mathbf{x}}{L}, \tag{42b}$$

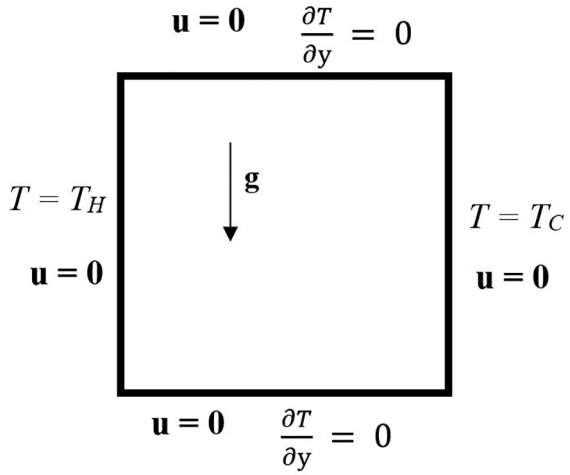

FIG. 2. Schematic for the natural convection of nanofluid in a cavity.

$$p' = \frac{p}{\rho_f U^2}, \quad t' = \frac{t\,U}{L}, \quad \boldsymbol{\tau}' = \frac{\boldsymbol{\tau}}{K\left(\frac{U}{L}\right)^m}, \tag{42c}$$

$$T' = (T - T_C)/\Delta T, \quad \Delta T = T_H - T_C. \tag{42d}$$

Based on the above non-dimensional variables, the non-dimensional equations are defined as[66–71]

$$\nabla \cdot \mathbf{u}' = 0, \tag{43}$$

$$\bar{\rho}\left[\frac{\partial \mathbf{u}'}{\partial t'} + (\mathbf{u}' \cdot \nabla)\,\mathbf{u}'\right] = -\nabla p' + \frac{1}{\sqrt{Gr}}\,\nabla \cdot \boldsymbol{\tau}' + \bar{\rho}\bar{\beta}T'\mathbf{e}_y, \tag{44}$$

$$\bar{\rho}\bar{c}\left[\frac{\partial T'}{\partial t'} + \mathbf{u}'.\nabla T'\right] = \frac{\bar{k}}{Pr\,Gr^{\frac{1}{m+1}}}\nabla^2 T'. \tag{45}$$

Grashof (Gr), Prandtl (Pr), and Rayleigh (Ra) numbers are obtained as

$$Gr = \frac{{\rho_f}^2 L^3 g\,\beta_f\,\Delta T}{\mu_r^2}, \quad Pr = \frac{\mu_r\,c_f}{k_f}, \quad Ra = Gr \times Pr, \tag{46}$$

where μ_r is the reference viscosity, and with considering the relation of $\dot{\gamma} \sim U/L$, it is found as

$$\mu_r \sim K\dot{\gamma}^{(m-1)} \sim K(U/L)^{(m-1)} \sim K\left(\sqrt{g\beta_f \Delta T L}/L\right)^{(m-1)}, \tag{47}$$

with the above definition, the Grashof number is modified as

$$Gr = \frac{{\rho_f}^2 L^{m+2}\,(g\,\beta_f\,\Delta T)^{2-m}}{K^2}. \tag{48}$$

The non-dimensional variables of f_α^{eq} in (9) with considering the non-dimensional macroscopic equations of (43)–(44) are defined as

$$A_0 = \bar{\rho} - \frac{2p'}{\sigma^2} - \frac{\bar{\rho}\,|\mathbf{u}'|^2}{\sigma^2}, \quad A_\alpha = 0, \quad \alpha = 1, \ldots, 8, \tag{49}$$

and

$$\Gamma_\alpha = \frac{\bar{\rho}\,\mathbf{u}'}{2\sigma^2}, \quad \alpha = 1,3,5,7; \quad \Gamma_\alpha = \mathbf{0}, \quad \alpha = 2,4,6,8. \tag{50}$$

Next,

$$\Lambda_{11} = \frac{1}{2\sigma^4}\left(p' + \bar{\rho}u'^2 - \frac{1}{\sqrt{Gr}}\tau'_{xx}\right), \tag{51}$$

$$\Lambda_{22} = \frac{1}{2\sigma^4}\left(p' + \bar{\rho}v'^2 - \frac{1}{\sqrt{Gr}}\tau'_{yy}\right), \tag{52}$$

and

$$\Lambda_{12} = \Lambda_{21} = \frac{1}{8\sigma^4}\left(\bar{\rho}\,u'v' - \frac{1}{\sqrt{Gr}}\tau'_{xy}\right), \tag{53}$$

where the non-dimensional extra tensors are calculated as

$$\tau'_{xx} = 2\dot{\gamma}'^{(m-1)}\left(\frac{\partial u'}{\partial x'}\right), \tag{54}$$

$$\tau'_{xy} = \tau'_{yx} = \dot{\gamma}'^{(m-1)}\left(\frac{\partial u'}{\partial y'} + \frac{\partial v'}{\partial x'}\right), \tag{55}$$

$$\tau'_{yy} = 2\dot{\gamma}'^{(m-1)}\left(\frac{\partial v'}{\partial y'}\right), \tag{56}$$

where

$$\dot{\gamma}' = \sqrt{2\left[\left(\frac{\partial v'}{\partial y'}\right)^2 + \left(\frac{\partial u'}{\partial x'}\right)^2\right] + \left(\frac{\partial u'}{\partial y'} + \frac{\partial v'}{\partial x'}\right)^2}. \tag{57}$$

The force term F_α, which is shown in (16) for this problem, is calculated as

$$F_\alpha = 0, \quad \alpha = 0, 2, 4, 6, 8, \tag{58a}$$

$$F_\alpha = \frac{1}{2\sigma^2}\left(\bar{\rho}\,\bar{\beta}\,T'\mathbf{e_y}\right)\cdot\mathbf{e}_\alpha, \quad \alpha = 1, 3, 5, 7. \tag{58b}$$

To find the elements of g_α^{eq} in (18), applying the non-dimensional energy equations of (45) is calculated by

$$D_\alpha = (\bar{\rho}\,\bar{c})T', \quad \alpha = 0; \quad D_\alpha = 0, \quad \alpha = 1, \ldots, 8, \tag{59}$$

and

$$\mathbf{E}_\alpha = \frac{1}{2\sigma^2}\left[(\bar{\rho}\bar{c})\mathbf{u}'T' - \frac{\bar{k}}{Pr\,Gr^{\frac{1}{m+1}}}\nabla T'\right], \quad \alpha = 1, 3, 5, 7, \tag{60}$$

$$\mathbf{E}_\alpha = \mathbf{0}, \quad \alpha = 0, 2, 4, 6, 8, \tag{61}$$

where $G_\alpha = 0$ in all directions. To validate the current method for the nanofluid effect on heat transfer, the results are compared with the study of Khanafer *et al.*[7] for Newtonian fluids ($m = 1$) where they investigated the natural convection of nanofluid, using the single model in a square enclosure for various volume fractions and Grashof numbers. The carrier fluid was water, and the nanoparticles were copper (the physical parameters are presented in the Table I). The viscosity and the thermal conductivity were volume fraction-dependent and followed the Brinkman and Maxwell–Garnett models. The temperature in the middle of the cavity at $y' = 0.5$ for $\phi = 0.1$ in different Grashof numbers are compared and presented in Fig. 3. The Nusselt number on the high temperature wall is considered as the criteria for the assessment of the heat transfer. The local (Nu_l) and the average (Nu) Nusselt numbers are defined by

$$Nu_l = \left(-\frac{\partial T'}{\partial x'}\right)_{x'=0}, \quad Nu = \int_0^1 Nu_l\, dy'. \tag{62}$$

Figure 4 demonstrates the values of Nu in different Grashof numbers and volume fractions for this study and the Khanafer *et al.*[7] ones. It shows a good agreement between two studies. To validate the accuracy of the presented code for non-Newtonian fluids, the natural convection of power-law fluid results is compared with reported results of Kim *et al.*[66] and Khezzar *et al.*[69] Table II illustrates and compares the ratio of the average Nusselt number $Nu^* = \frac{Nu_{m=m}}{Nu_{m=1}}$ in various power-law indexes at $Ra = 10^5$ and $Pr = 100$. The applied mesh for this case is $\Delta x = \Delta y = \frac{1}{150}$ and the time step is $\Delta t = 10^{-4}$ with considering the shown stability in Appendix A.

It is reported[60–65] that the non-Newtonian nanofluids usually show shear-thinning behavior ($m < 1$). In addition, we approximate the power-law index is a constant value and the results (streamlines

TABLE I. Thermophysical properties of water, copper (Cu), alumina (Al_2O_3), and ethylene glycol (EG).

Property	Water	Cu	Al_2O_3	EG
c (J/kg K)	4179	383	765	2415
ρ (kg/m^3)	997.1	8954	3970	1114
k (W/m K)	0.6	400	40	0.252
$\beta \times 10^5$ (K^{-1})	21	1.67	0.8	57

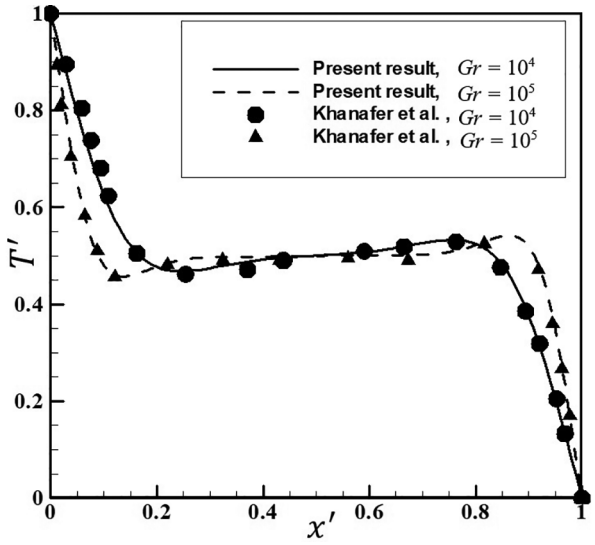

FIG. 3. Temperature comparison at $y' = 0.5$ between present study and the results of Khanafer *et al.*[7] for $\phi = 0.1$.

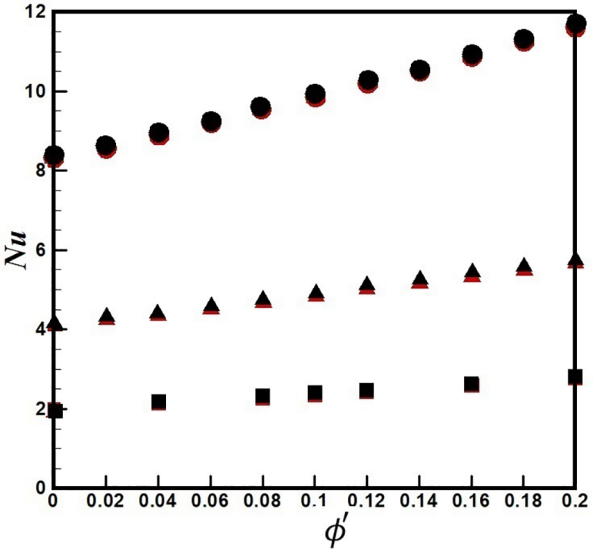

FIG. 4. Comparison of the average Nusselt number between present study (Black) and the results of Khanafer *et al.*[7] (red) at $Gr = 10^3$(□), $Gr = 10^4$(△), $Gr = 10^5$(○).

TABLE II. Comparisons of Nu^* for different power-law indexes m at $Ra = 10^5$ and $Pr = 100$.

m	0.6	0.8	1	1.2	1.4
Present study	1.49	1.19	1	0.88	0.81
Kim *et al.*[66]	1.46	1.17	1	...	...
Khezzar *et al.*[69]	1.48	1.18	1	0.89	0.82
Turan *et al.*[68]	1.49	1.19	1	...	...

and isotherms) are presented at Fig. 5 for power-law index of $m = 0.6$ at $Ra = 10^4$ in the volume fractions of $\phi = 0$ and $\phi = 0.06$. It demonstrates that the addition of nanoparticles strengthens the convection process with the enhancement of the movement of isotherms and the expansion of streamlines. The temperature and the velocities in the middle of the cavity in Figs. 6–8 also confirm the behavior where the curvature, which presents the rise of heat transfer, augments with the enhancement of volume fraction gradually. The average Nusselt numbers for the studied power-law indexes are shown in Fig. 9 for various volume fractions at $Ra = 10^4$. It is clear that the increase in the volume fraction enhances the average Nusselt number steadily in various power-law indexes.

Two-phase model

The natural convection of nanofluid (see, Fig. 2), using a two-phase model based on the dimensional equations (3)–(6) is solved, using the present method. It should be noted that the nanoparticle diffusion mass flux on the boundaries is zero ($\mathbf{j} = 0$). The non-dimensional equations with using the shown non-dimensional parameters in the single-phase example and introducing non-dimensional variables in the nanoparticle equation by $\phi' = \phi/\phi_a$, where ϕ_a is the average volume fraction, which is found based on the densities of solid particles and fluid with considering the temperature[19] are presented as

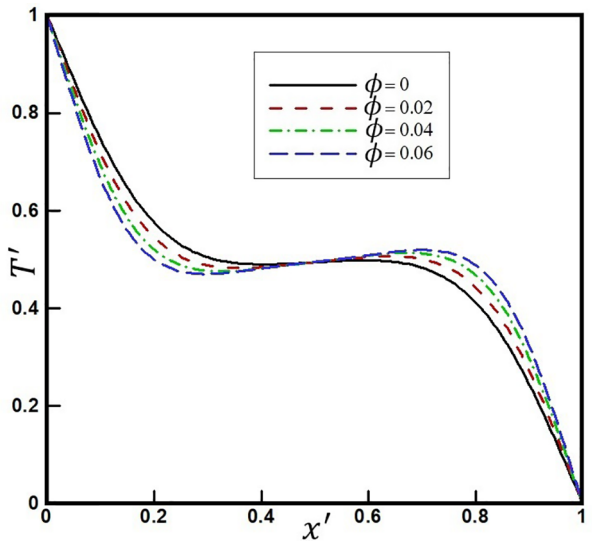

FIG. 6. The non-dimensional temperature (T') in the middle of the cavity ($y' = 0.5$) for different volume fractions at $m = 0.6$ and $Ra = 10^4$.

$$\nabla \cdot \mathbf{u}' = 0, \tag{63}$$

$$\bar{\rho}\left[\frac{\partial \mathbf{u}'}{\partial t'} + (\mathbf{u}' \cdot \nabla)\,\mathbf{u}'\right] = -\nabla p' + \frac{1}{\sqrt{Gr}}\nabla \cdot \boldsymbol{\tau}' + \bar{\rho}\bar{\beta}T'\mathbf{e}_y, \tag{64}$$

$$\bar{\rho}\bar{c}\left[\frac{\partial T'}{\partial t'} + \mathbf{u}'.\nabla T'\right] = \frac{1}{Pr\,Gr^{\frac{1}{m+1}}}\left[\bar{k}\nabla^2 T' + \frac{1}{Le}\nabla T' \cdot \nabla \phi' + \frac{1}{Le\,N_{BT}}\nabla T' \cdot \nabla T'\right], \tag{65}$$

$$\left[\frac{\partial \phi'}{\partial t'} + \mathbf{u}'.\nabla \phi'\right] = \frac{1}{Le\,Pr\,Gr^{\frac{1}{m+1}}}\left[\frac{\nabla^2 T'}{N_{BT}} + \nabla^2 \phi'\right]. \tag{66}$$

Lewis number (Le) and N_{BT} are defined as

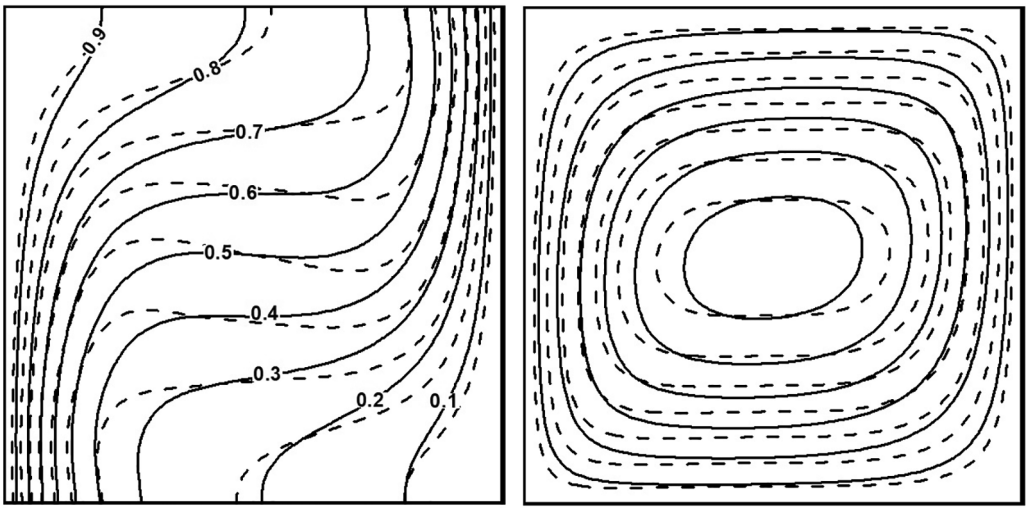

FIG. 5. Streamlines (the right contour) and isotherms (the left contour) at $m = 0.6$, $Ra = 10^4$ for $\phi = 0$ (–) and $\phi = 0.06$ (– –).

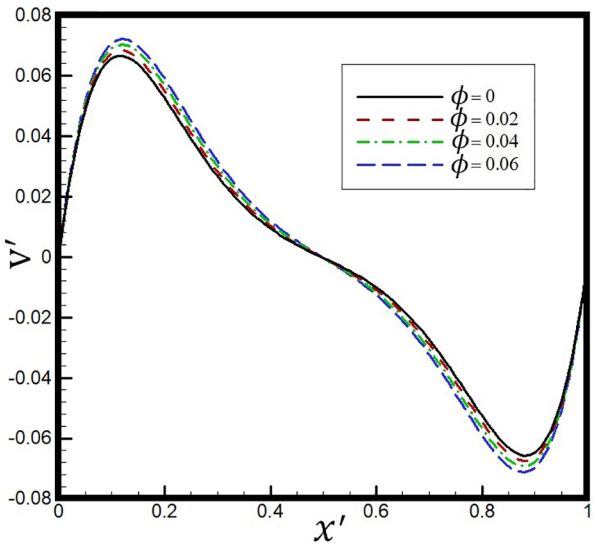

FIG. 7. The non-dimensional vertical velocity (v′) in the middle of the cavity ($y' = 0.5$) for different volume fractions at $m = 1$ and $Ra = 10^4$.

$$Le = \frac{k_f}{\rho_p c_p D_B \phi_a}, \quad N_{BT} = \frac{N_b}{N_t}, \tag{67}$$

where N_{BT} is the ratio of the non-dimensional variables of Brownian motion (N_b) and Thermophoresis parameter (N_t), which are calculated as

$$N_b = \frac{\rho_p c_p D_B \phi_a}{k_f}, \quad N_t = \frac{\rho_p c_p D_T \Delta T}{k_f T_C}. \tag{68}$$

The non-dimensional variables of f_α^{eq} to satisfy the equations of (63) and (64) for the two-phase model are similar to the equations of (49)

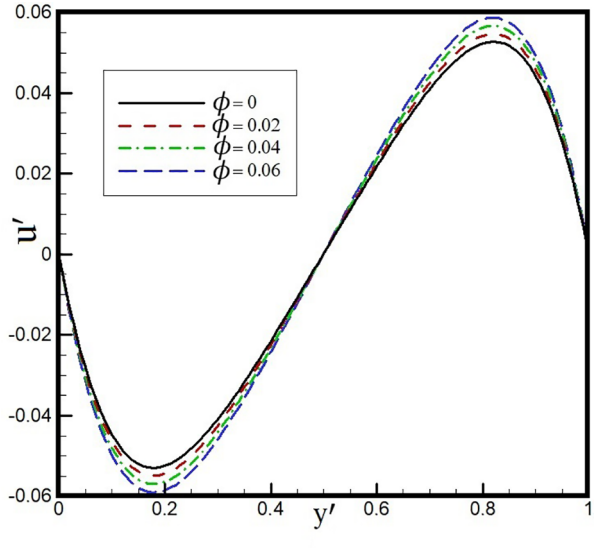

FIG. 8. The non-dimensional horizontal velocity (u′) in the middle of the cavity ($x' = 0.5$) for different volume fractions at $m = 1$ and $Ra = 10^4$.

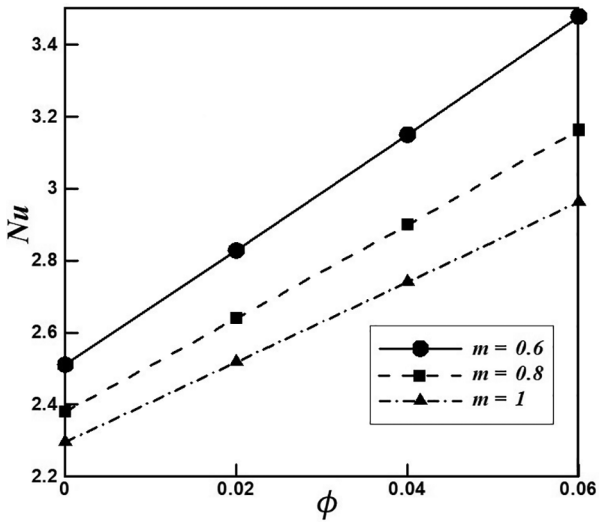

FIG. 9. The average Nusselt number for different power-law indexes and volume fractions at $Ra = 10^4$.

and (50). In addition, the shown force term in the equation is the same as (58a) and (58b). The parameters of g_α^{eq} are found by

$$D_\alpha = \bar{\rho}\bar{c}T', \quad \alpha = 0; \quad D_\alpha = 0, \quad \alpha = 1, \ldots, 8, \tag{69}$$

and for $\alpha = 1, 3, 5, 7$

$$\mathbf{E}_\alpha = \frac{1}{2\sigma^2}\left[\bar{\rho}\bar{c}\mathbf{u}'T' - \frac{1}{Pr\,Gr^{\frac{1}{m+1}}}\left(\bar{k}\nabla T' + \frac{1}{Le}T'\nabla\phi' + \frac{1}{Le N_{BT}}\nabla T'\right)\right], \tag{70}$$

$$\mathbf{E}_\alpha = \mathbf{0}, \quad \alpha = 0, 2, 4, 6, 8, \tag{71}$$

and G_α is calculated by

$$G_\alpha = -\frac{1}{Le}T'\nabla^2\phi' - \frac{1}{Le\,N_{BT}}\nabla^2 T', \quad \alpha = 1, 3, 5, 7, \tag{72}$$

$$G_\alpha = 0, \quad \alpha = 0, 2, 4, 6, 8. \tag{73}$$

To achieve the non-dimensional equations of nanoparticles, the parameters of s_α^{eq} are written by

$$\Pi_\alpha = \begin{cases} \phi', & \alpha = 0, \\ \mathbf{0}, & \alpha = 1, \ldots, 8, \end{cases} \tag{74}$$

and for $\alpha = 1, 3, 5, 7$, we have

$$\mathbf{\Omega}_\alpha = \frac{1}{2\sigma^2}\left[\mathbf{u}'\phi' - \frac{1}{Le\,Pr\,Gr^{\frac{1}{m+1}}}\left(\frac{1}{N_{BT}}\nabla T' + \nabla\phi'\right)\right], \tag{75}$$

but $\mathbf{\Omega}_\alpha = 0$ at $\alpha = 0, 2, 3, 6, 8$. It is clear that if $N_t = N_b = 0$, the momentum and energy equations generate the results of the single-phase model. The same mesh and time step of single-phase model are used here ($\Delta x = \Delta y = \frac{1}{150}$, $\Delta t = 10^{-4}$). The natural convection of Newtonian ($m = 1$) nanofluid of alumina–water (the physical parameters are presented in the Table I) using the two-phase model was studied by Corcione *et al.*,[22] while they neglected the effects of Brownian and thermophoretic in the energy equation (65) and just

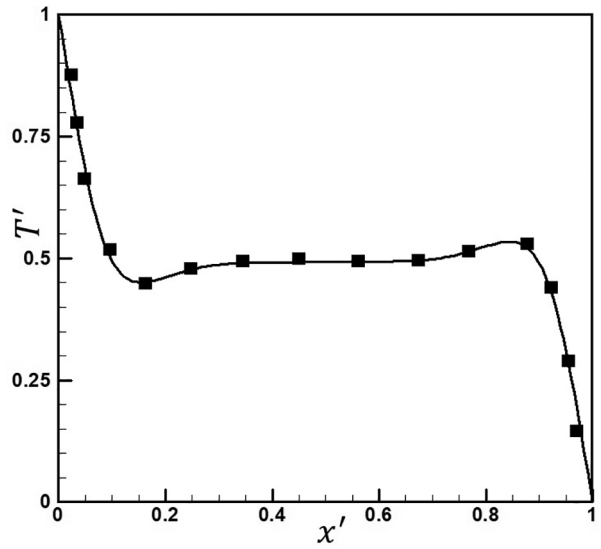

FIG. 10. The comparison of temperature distribution in the middle of the cavity between current code (–) and the results of Corcione *et al.*[22] (□) for $d_p = 25$ nm, and $\phi_a = 0.04$.

considered their influence in the format of their ratio (N_{BT}) in the nanoparticle equation (in Ref. 19 was mentioned, we can ignore the parameters in the energy equation in this case due to the high values of $Le\,N_{BT}$). In fact, the single-phase energy equation was applied in Ref. 22. They used temperature- and the nanoparticle diameter-dependent properties in their study as

$$\bar{k} = 1 + 4.4\,Re_n^{0.4} Pr^{0.66} \left(\frac{T}{T_{fr}}\right)^{10} \left(\frac{k_p}{k_f}\right)^{0.03} \phi^{0.66}. \tag{76}$$

T_{fr} is the freezing point of the base fluid (for this case, it is water) at T_C (which was considered at $T_C = 293$ K) and the nanoparticle Reynolds number (Re_n) was defined as

$$Re_n = \frac{2\rho_f k_B T}{\pi \mu_f{}^2 d_p} \tag{77}$$

and

$$\frac{\mu_n}{\mu_f} = \frac{1}{1 - 34.87(d_p/d_f)^{-0.3}\phi^{1.03}}, \tag{78}$$

where d_f is the equivalent diameter of the base fluid molecule at T_C and calculated by

$$d_f = 0.1\left[\frac{6M}{N\pi\rho_m}\right]^{1/3}. \tag{79}$$

Here, N, M, ρ_m are the constant Avogadro number, the molar mass, and the mass density at T_C for the carrier fluid, respectively. In Fig. 10, the temperature distribution in the middle of the cavity is compared and validated with the study of Ref. 22 for the case of $d_p = 25$ nm, and $\phi_a = 0.04$ [it should be noted that in Ref. 22 for this case, the temperature difference of $\Delta T = 10$ K (305–315 K) and the cavity length of $L = 0.01$ were applied]. The streamlines and isotherms are also validated for the mentioned problem in Fig. 11, which demonstrates a good agreement with the results of Ref. 22 (for the considered parameters, the equal Rayleigh number is $Ra = 3.37 \times 10^5$). The applied mesh for this simulation is $\Delta x = \Delta y = \frac{1}{300}$, and the time interval is $\Delta t = 10^{-4}$. Figure 12 depicts the residual of the difference between the distribution function and the density of nanofluid ($|\rho_n - \sum_{i=0}^{8} f_i(\mathbf{x}, t)| < \delta$) against the number of iteration for the case study. It demonstrates that the code is converged with the criteria of $\delta = \Delta t^2$ close to 9×10^5 iteration.

It was reported by Minakov *et al.*[16] that the nanofluid of ethylene glycol and alumina in small particle sizes [$d_p \leq 50$ nm] shows non-Newtonian power-law model with different ranges of power-law indexes from $m = 0.572$ to $m = 0.850$ in different particle sizes. To simulate the non-Newtonian nanofluid of ethylene glycol and alumina with the two-phase model with considering the reported values for $d_p = 10$ nm, $\phi_a = 0.04$, and $\Delta T = 10$ K, the parameters are

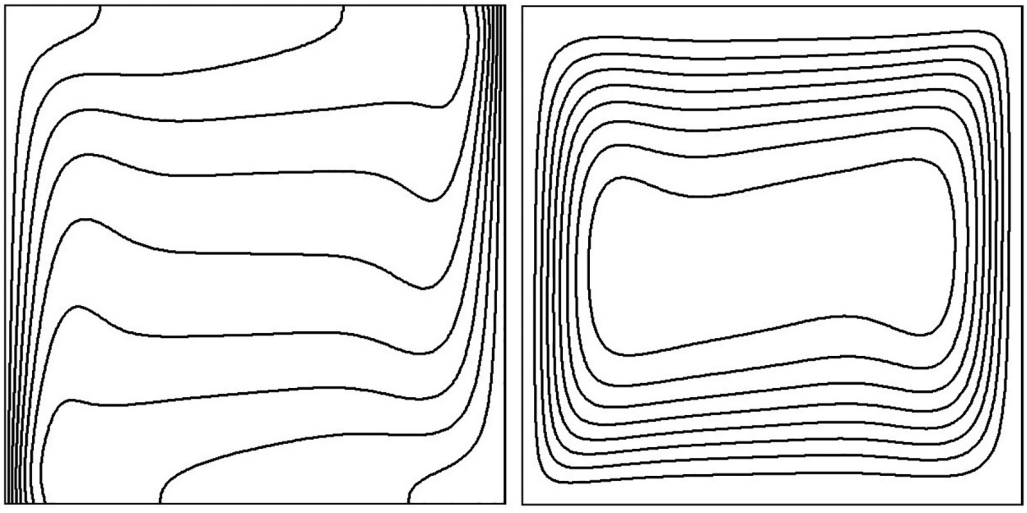

FIG. 11. The streamlines (the right contour) and isotherms (the left contour) for $d_p = 25$ nm, and $\phi_a = 0.04$.

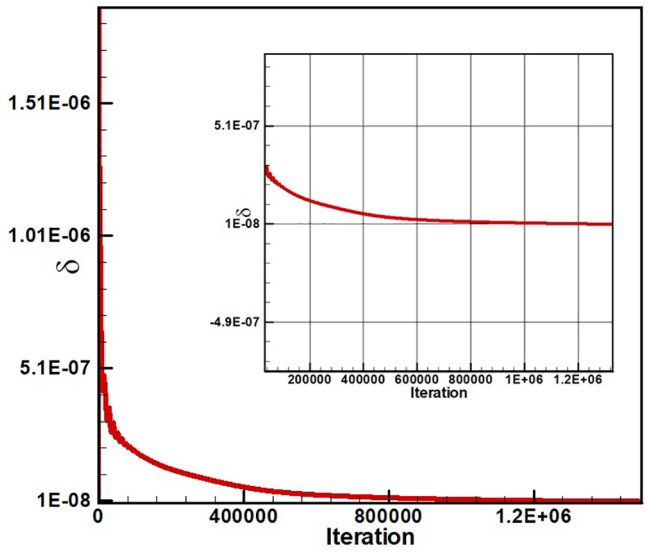

FIG. 12. The residual of the difference between the distribution function and the density of nanofluid against the number of iteration.

considered at $Le = 10^4$ and $N_{BT} = 0.2$ for different Grashof numbers of $Gr = 10^3, 5 \times 10^3, 10^4$ and fixed power-law indexes of $m = 0.6$, 0.8, and 1. In Fig. 13, the streamlines, isotherms, and nanoparticle distribution of the studied case are provided for the power-law indexes of $m = 0.6$ and $m = 1$ at $Gr = 5 \times 10^3$. It is shown that the convection intensity strengthens as the power-law index declines, which is observed in the isotherms and streamlines clearly. The nanoparticle distribution behaves similarly in the both power-law indexes, and it is the same as the reported nanoparticle concentration contour in Ref. 22, where the maximum and minimum values of volume fractions are concentrated on the walls of the cavity and nanoparticles are aggregated symmetrically. The average Nusselt number ratio ($Nu^* = \frac{Nu_{m=m}}{Nu_{m=1}}$) for evaluated power-law indexes and Grashof numbers is depicted in Fig. 14. It shows that the influence of nanoparticles enhances with the rise of Grashof numbers and drop of power-law index. The Sherwood number is a criterion for studying mass transfer where the local (Sh_l) and the average (Sh) Sherwood numbers are defined by

$$Sh_l = \left(-\frac{\partial \phi'}{\partial x'}\right)_{x'=0}, \quad Sh = \int_0^1 Sh_l \, dy'. \tag{80}$$

Since the boundary condition of zero total mass flux ($\mathbf{j} = 0$) is selected on the hot wall ($x' = 0$), the following relation on the hot wall is obtained as

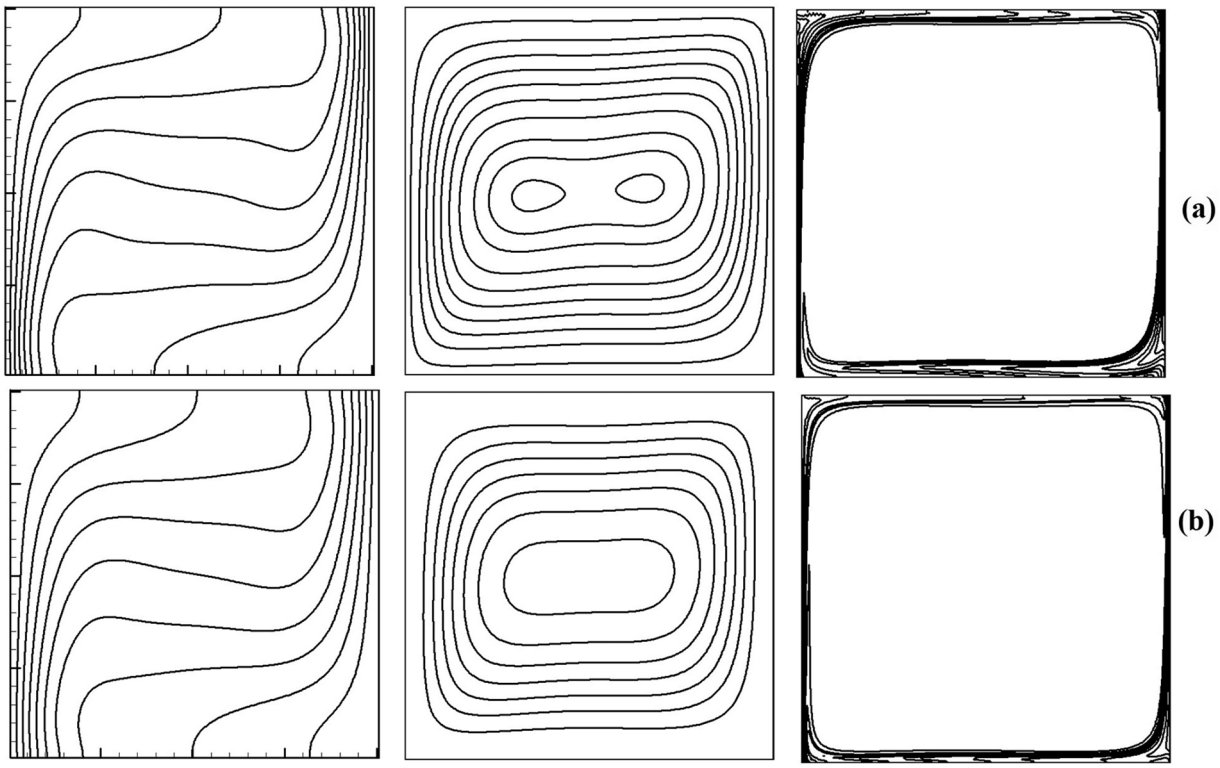

FIG. 13. The isotherms (the first column), the streamlines (the second column), and the nanoparticles distribution (the right column) at $d_p = 25$ nm, $\phi_a = 0.04$, $Gr = 5 \times 10^3$ for (a) $m = 0.6$ and (b) $m = 1$.

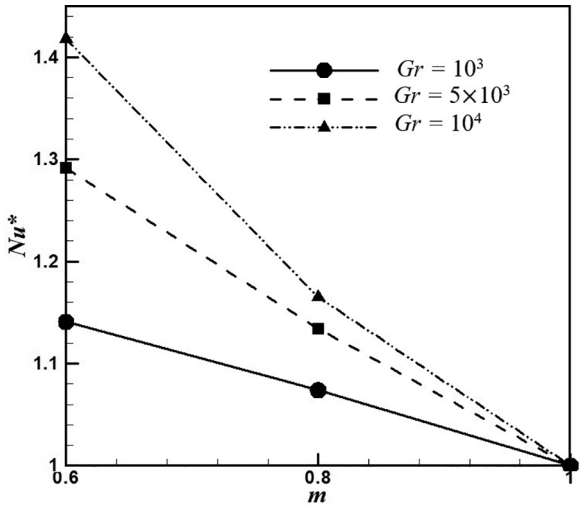

FIG. 14. The average Nusselt number ratio (Nu^*) in different power-law indexes for $d_p = 25\,\text{nm}$, and $\phi_a = 0.04$ at $Gr = 10^3(\bigcirc)$, $Gr = 5 \times 10^3(\square)$, $Gr = 10^4(\triangle)$.

$$\frac{\partial \phi'}{\partial x'} = -\frac{1}{N_{BT}} \frac{\partial T'}{\partial x'}. \tag{81}$$

So, the local and average Sherwood numbers can be found through the Nusselt number as

$$Sh_l = \frac{1}{N_{BT}} Nu_l, \quad Sh = \frac{1}{N_{BT}} Nu. \tag{82}$$

The local Sherwood number (Sh_l) on the hot wall for different power-law indexes is presented in Fig. 15 for $d_p = 25\,(nm)$, $Gr = 10^4$, $N_{BT} = 0.2$, and $\phi_a = 0.04$. It demonstrates Sh_l decreases gradually with the rise of power-law index, and the maximum difference of this value in the studied power-law index is observed close to the horizontal bottom wall. The average Nusselt number also is calculated and shown in Fig. 16 at $d_p = 25\,\text{nm}$, and $\phi_a = 0.04$ for various Grashof numbers and power-law indexes. As it was expected, it follows the same behavior of the average Nusselt number with a factor of N_{BT}.

B. Viscoplastic nanofluid

In some cases of nanofluids, a viscoplastic behavior was observed.[16] In addition, in some studies, the effects of nanoparticles on heat transfer are studied in viscoplastic fluids.[17,18] In viscoplastic material, it flows like a regular fluid when the yield stress (τ_y) is higher or equal to the magnitude of the extra stress tensor ($\boldsymbol{\tau}$) (in this case, this part is known yielded) and it remains solid or move in a rigid format when the yield stress is less than the magnitude of the extra stress tensor (in this case, this part is known unyielded).[72] Multifarious models and approximations are suggested and introduced for the viscoplastic fluids, but in most experimental non-Newtonian nanofluids cases, for example, the ethylene glycol nanofluids have shown a Herschel–Bulkley (HB) pattern, which also covers the shear thinning trend of nanofluids.[16,73–75] The HB model is defined as[72]

$$\begin{cases} \mathbf{A} = \mathbf{0}, & |\boldsymbol{\tau}| \le \tau_y, \\ \boldsymbol{\tau} = \left(K_H \dot{\gamma}^{(m-1)} + \dfrac{\tau_y}{\dot{\gamma}}\right)\mathbf{A}, & |\boldsymbol{\tau}| > \tau_y. \end{cases} \tag{83}$$

K_H is the consistency factor for the HB model and $|\boldsymbol{\tau}|$ is defined by

$$|\boldsymbol{\tau}| = \sqrt{\frac{1}{2}\boldsymbol{\tau} : \boldsymbol{\tau}}. \tag{84}$$

One model, which is utterly equivalent to the HB model, is introducing a traceless tensor ($\mathbf{II}$)[72] in the model to distinguish the yielded and

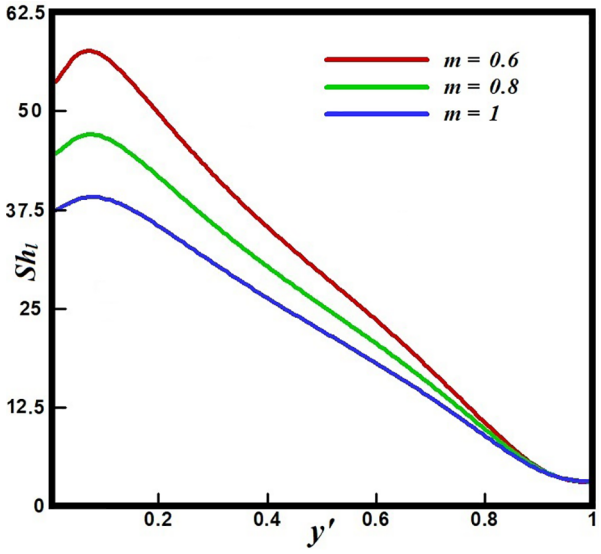

FIG. 15. The local Sherwood number (Sh_l) in different power-law indexes for $d_p = 25\,\text{nm}$, $Gr = 10^4$, and $\phi_a = 0.04$.

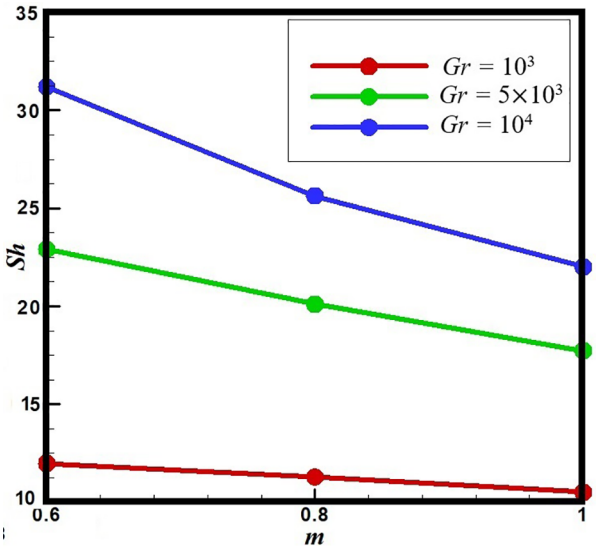

FIG. 16. The average Sherwood number (Sh) in different power-law indexes and Grashof numbers for $d_p = 25\,\text{nm}$ and $\phi_a = 0.04$.

unyielded regions, which has been applied here for the HB model as[72,76–78]

$$\boldsymbol{\tau} = K_H\,\dot{\gamma}^{(m-1)}\mathbf{A} + \sqrt{2}\,\tau_y\,\mathbf{II}, \quad \mathbf{1}:\mathbf{II} = 0. \tag{85}$$

The traceless tensor is called the *viscoplasticity constraint tensor* and is discussed in detail in Refs. 72 and 76–78. Appendix E explains the conditions and process of obtaining the tensor.

To study the viscoplastic nanofluid using the two-phase model, the benchmark of natural convection is investigated (see Fig. 2) with the mentioned boundary conditions. The non-dimensional parameters are similar to (42a)–(42d) and are written as

$$\hat{\rho} = \frac{\rho_n}{\rho_f}, \quad \hat{c} = \frac{c_n}{c_f}, \quad \hat{k} = \frac{k_n}{k_f}, \quad \hat{\beta} = \frac{\beta_n}{\beta_f}, \tag{86a}$$

$$U = \sqrt{g\beta_n \Delta T L}, \quad \hat{\mathbf{u}} = \frac{\mathbf{u}}{U}, \quad \hat{\mathbf{x}} = \frac{\mathbf{x}}{L}, \tag{86b}$$

$$\hat{p} = \frac{p}{\rho_f\,U^2}, \quad \hat{t} = \frac{t\,U}{L}, \quad \hat{\boldsymbol{\tau}} = \frac{\boldsymbol{\tau}}{K_H\left(\frac{U}{L}\right)^m}, \tag{86c}$$

$$\hat{T} = \frac{(T - T_C)}{\Delta T}, \quad \Delta T = T_H - T_C, \quad \hat{\phi} = \frac{\phi}{\phi_a}. \tag{86d}$$

So, the non-dimensional equations are generated similar to (63)–(66) as

$$\nabla\cdot\hat{\mathbf{u}} = 0, \tag{87}$$

$$\hat{\rho}\left[\partial\frac{\hat{\mathbf{u}}}{\partial}\hat{t} + (\hat{\mathbf{u}}\cdot\nabla)\,\hat{\mathbf{u}}\right] = -\nabla\hat{p} + \frac{1}{\sqrt{Gr}}\,\nabla\cdot\hat{\boldsymbol{\tau}} + \hat{\rho}\hat{\beta}\hat{T}\mathbf{e_y}, \tag{88}$$

$$\hat{\rho}\hat{c}\left[\frac{\partial\hat{T}}{\partial\hat{t}} + \hat{\mathbf{u}}.\nabla\hat{T}\right] = \frac{1}{Pr\,Gr^{\frac{1}{m+1}}}\left[\hat{k}\nabla^2\hat{T} + \frac{1}{Le}\,\nabla\hat{T}\cdot\nabla\hat{\phi} + \frac{1}{Le\,N_{BT}}\,\nabla\hat{T}\cdot\nabla\hat{T}\right], \tag{89}$$

$$\left[\frac{\partial\hat{\phi}}{\partial\hat{t}} + \hat{\mathbf{u}}.\nabla\hat{\phi}\right] = \frac{1}{Le\,Pr\,Gr^{\frac{1}{m+1}}}\left[\frac{\nabla^2\hat{T}}{N_{BT}} + \nabla^2\hat{\phi}\right]. \tag{90}$$

The non-dimensional parameters follow the definitions of the power-law model as

$$Gr = \frac{{\rho_f}^2\,L^{m+2}\,(g\,\beta_f\,\Delta T)^{2-m}}{{K_H}^2}, \tag{91}$$

$$Pr = \frac{c_f\,K_H\left(\sqrt{g\beta_f\Delta T L}/L\right)^{(m-1)}}{k_f}, \tag{92}$$

$$Le = \frac{k_f}{\rho_p c_p D_B \phi_a}, \quad N_{BT} = \frac{D_B\phi_a T_C}{D_T\Delta T}. \tag{93}$$

As it was mentioned, the non-dimensional equilibrium distribution lattice function (f_α^{eq}) can be defined as

$$f_\alpha^{eq} = A_\alpha + \mathbf{e}_\alpha\cdot\Gamma_\alpha + (\mathbf{e}_\alpha\otimes\mathbf{e}_\alpha):\Lambda_\alpha, \tag{94}$$

$$A_0 = \hat{\rho} - \frac{2\hat{p}}{\sigma^2} - \frac{\hat{\rho}\,|\hat{\mathbf{u}}|^2}{\sigma^2}, \quad A_\alpha = 0, \quad \alpha = 1,\ldots,8, \tag{95}$$

and

$$\Gamma_\alpha = \hat{\rho}\,\frac{\hat{\mathbf{u}}}{2\sigma^2}, \quad \alpha = 1,3,5,7; \quad \Gamma_\alpha = \mathbf{0}, \quad \alpha = 2,4,6,8. \tag{96}$$

Next,

$$\begin{aligned}\Lambda_{11} &= \frac{1}{2\sigma^4}\left(\hat{p} + \hat{\rho}\hat{u}^2 - \frac{1}{\sqrt{Gr}}\hat{\tau}_{xx}\right),\\ \Lambda_{22} &= \frac{1}{2\sigma^4}\left(\hat{p} + \hat{\rho}\hat{v}^2 - \frac{1}{\sqrt{Gr}}\hat{\tau}_{yy}\right),\end{aligned} \tag{97}$$

and

$$\Lambda_{12} = \Lambda_{21} = \frac{1}{8\sigma^4}\left(\hat{\rho}\,\hat{u}\hat{v} - \frac{1}{\sqrt{Gr}}\hat{\tau}_{xy}\right). \tag{98}$$

In fact, the parameters of f_α^{eq} are like the equations of (49)–(53), but the extra stress tensors are calculated by

$$\hat{\tau}_{xx} = 2\,\dot{\gamma}''^{(m-1)}\left(\frac{\partial\hat{u}}{\partial\hat{x}}\right) + \sqrt{2}\,Bn\,\mathbf{II}_{xx}, \tag{99}$$

$$\hat{\tau}_{yy} = 2\,\dot{\gamma}''^{(m-1)}\left(\frac{\partial\hat{v}}{\partial\hat{y}}\right) + \sqrt{2}\,Bn\,\mathbf{II}_{yy}, \tag{100}$$

$$\hat{\tau}_{xy} = \dot{\gamma}''^{(m-1)}\left(\frac{\partial\hat{u}}{\partial\hat{y}} + \frac{\partial\hat{v}}{\partial\hat{x}}\right) + \sqrt{2}\,Bn\,\mathbf{II}_{xy}, \tag{101}$$

where the non-dimensional parameter of Bingham number is written as

$$Bn = \frac{\tau_y\,L^m}{K_H\,U^m} \tag{102}$$

and

$$\dot{\gamma}'' = \sqrt{2\left[\left(\frac{\partial\hat{v}}{\partial\hat{y}}\right)^2 + \left(\frac{\partial\hat{u}}{\partial\hat{x}}\right)^2\right] + \left(\frac{\partial\hat{u}}{\partial\hat{y}} + \frac{\partial\hat{v}}{\partial\hat{x}}\right)^2}, \tag{103}$$

where the non-dimensional format of the projection operation between the two time steps of n and $n+1$ for obtaining the viscoplasticity constraint tensor in Appendix E is defined as

$$\mathbf{II}^{n+1} = PR_{\mathcal{M}}(\mathbf{II}^n + Bn\,Pr\,\mathbf{A}^n). \tag{104}$$

The force term and the parameters of g_α^{eq} and s_α^{eq} are the same as the presented equations in the case of power-law model for the two-phase model. The force term F_α, which is shown in (16) for this problem, is recalled as

$$F_\alpha = 0, \quad \alpha = 0,2,4,6,8, \tag{105a}$$

$$F_\alpha = \frac{1}{2\sigma^2}\left(\hat{\rho}\,\hat{\beta}\,\hat{T}\mathbf{e_y}\right)\cdot\mathbf{e}_\alpha, \quad \alpha = 1,3,5,7. \tag{105b}$$

To find the elements of g_α^{eq} in (18), applying the non-dimensional energy equations is calculated by

$$g_\alpha^{eq} = D_\alpha + \mathbf{e}_\alpha\cdot\mathbf{E}_\alpha, \tag{106}$$

$$D_\alpha = \hat{\rho}\hat{c}\hat{T}, \quad \alpha = 0; \quad D_\alpha = 0, \quad \alpha = 1,\ldots,8, \tag{107}$$

and for $\alpha = 1,3,5,7$

TABLE III. Comparison of the average Nusselt number (Nu) in different Bingham numbers for $Pr = 1$, $m = 1$, $Ra = 10^4$ and 10^5.

	$Bn = 0$	$Bn = 0.5$	$Bn = 1$	$Bn = 1.5$	$Bn = 2$	$Bn = 2.5$	$Bn = 3$
$Ra = 10^4$							
Turan *et al.*[79]	2.23	2.00	1.70	1.43	1.21	1.10	1.00
Huilgol and Kefayati[76]	2.23	1.91	1.65	1.49	1.34	1.21	1.1
Present study	2.22	1.94	1.67	1.46	1.28	1.16	1.05
$Ra = 10^5$							
Turan *et al.*[79]	4.60	···	3.89	···	3.45	···	2.95
Huilgol and Kefayati[76]	4.60	···	3.89	···	3.46	···	3.16
Present study	4.58	···	3.90	···	3.44	···	3.05

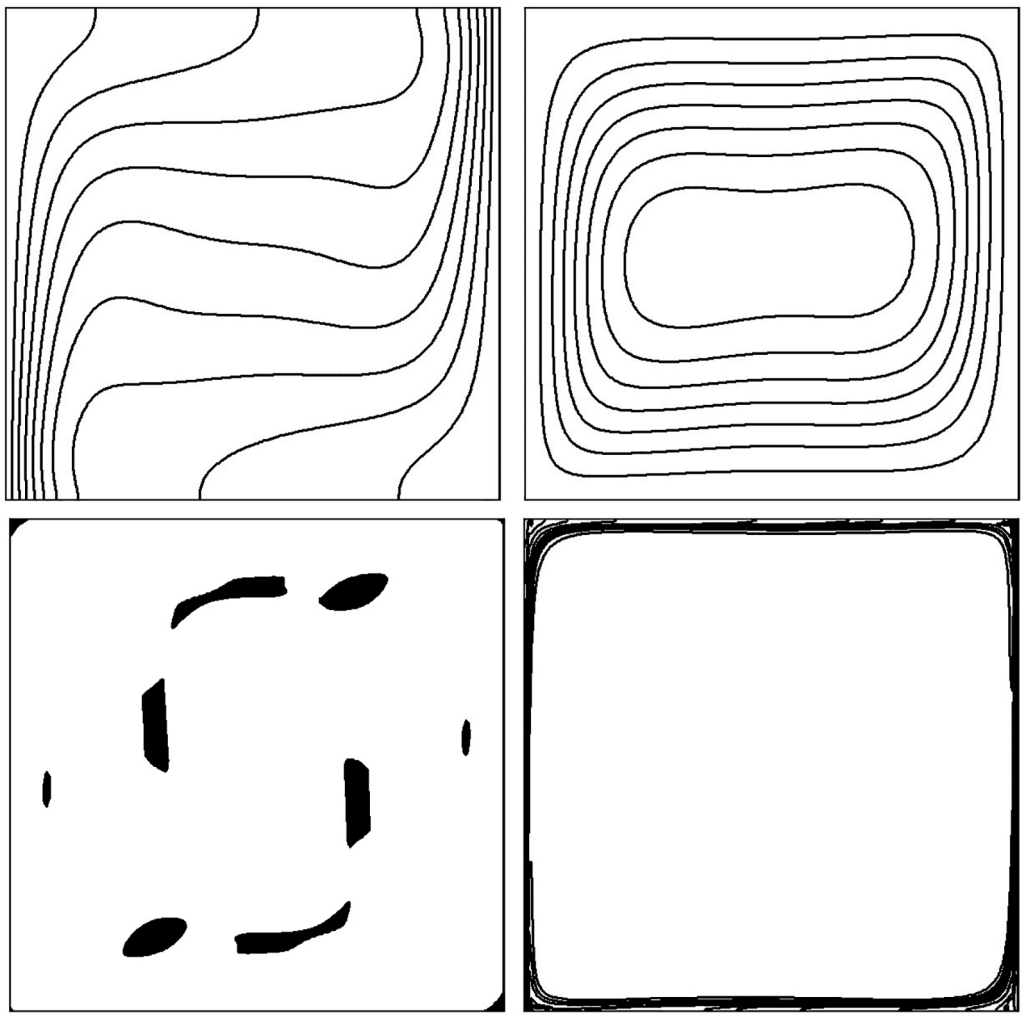

FIG. 17. The contours of isotherms (the top left), the streamlines (the top right), the yielded/unyielded (the bottom left), and the nanoparticles distribution (the bottom right) at $Gr = 10^4$, $\phi_a = 0.04$, and $Bn = 0.5$.

$$\mathbf{E}_\alpha = \frac{1}{2\sigma^2}\left[\hat{\rho}\hat{c}\hat{\mathbf{u}}\hat{T} - \frac{1}{Pr\,Gr^{\frac{1}{m+1}}}\left(\hat{k}\nabla\hat{T} + \frac{1}{Le}\hat{T}\nabla\hat{\phi} + \frac{1}{Le\,N_{BT}}\nabla\hat{T}\right)\right], \tag{108}$$

$$\mathbf{E}_\alpha = \mathbf{0}, \quad \alpha = 0, 2, 4, 6, 8, \tag{109}$$

and G_α is calculated by

$$G_\alpha = -\frac{1}{Le}\hat{T}\nabla^2\hat{\phi} - \frac{1}{Le\,N_{BT}}\nabla^2\hat{T}, \quad \alpha = 1, 3, 5, 7, \tag{110}$$

$$G_\alpha = 0, \quad \alpha = 0, 2, 4, 6, 8, \tag{111}$$

$$s_\alpha^{eq} = \Pi_\alpha + \mathbf{e}_\alpha \cdot \mathbf{\Omega}_\alpha. \tag{112}$$

To achieve the non-dimensional equations of nanoparticles, the parameters of s_α^{eq} are written by

$$\Pi_\alpha = \begin{cases} \hat{\phi}, & \alpha = 0, \\ \mathbf{0}, & \alpha = 1, \ldots, 8, \end{cases} \tag{113}$$

and for $\alpha = 1, 3, 5, 7$, we have

$$\mathbf{\Omega}_\alpha = \frac{1}{2\sigma^2}\left[\hat{\mathbf{u}}\hat{\phi} - \frac{1}{Le\,Pr\,Gr^{\frac{1}{m+1}}}\left(\frac{1}{N_{BT}}\nabla\hat{T} + \nabla\hat{\phi}\right)\right], \tag{114}$$

where $\mathbf{\Omega}_\alpha = 0$ at $\alpha = 0, 2, 3, 6, 8$. The code was used to study isothermal and thermal benchmark problems filling with viscoplastic fluids before in Refs. 77–85. The present HB model for natural convection of viscoplastic fluid is compared with reported results of Turan *et al.*[79] and Huilgol and Kefayati.[76] Table III depicts and compares the average Nusselt number in various Bingham numbers for $Pr = 1$, $m = 1$, $Ra = 10^4$ and 10^5.

For the volume fraction of $\phi_a = 0.04$ and $d_p = 11$ nm of ethylene glycol–alumina, viscoplastic HB behavior was observed[16] where the values of $\tau_y = 121.8$ mPa, $K_H = 57.67$ mPa s^m, and $m = 0.692$ were reported, so this case has been selected to be investigated in this benchmark for different Grashof numbers of $Gr = 10^3, 5 \times 10^3, 10^4$ and Bingham numbers of $Bn = 0.1, 0.5$ and 1 at $Le = 10^4$, $N_{BT} = 0.2$, and $\Delta T = 10$ K. The grid size of $\Delta x = \Delta y = \frac{1}{300}$ and the time step of $\Delta t = 10^{-4}$ are applied for this study. The contours of the studied case are shown in Fig. 17. It shows the maximum concentration of nanoparticles is present on the walls of the cavity similar to the shear-thinning case. In addition, the unyielded part (the black section) has a symmetric behavior similar to the reported trend for pure fluids in natural convection of viscoplastic fluids.[72,76–78] Figure 18 demonstrates that the increase in Bingham number, which has a direct relation with the yield stress, declines the convection process gradually and it is evident with the change of the temperature distribution behavior and decrease in the curvature of the profile. In Fig. 19, it is observed that the average Nusselt number declines steadily as the Bingham number rises in different Grashof numbers. The effect of Bingham number on the local velocity in the middle of the cavity is presented in Figs. 20 and 21, which illustrates the horizontal and vertical velocities drop gradually with the rise of Bingham number or the increase in the yield stress. The average Sherwood numbers can be found easily through the average Nusselt number with the multiplication of $1/N_{BT}$, so it can be displayed in the form of Fig. 22, so *Sh* shows the same trend of *Nu* against Bingham number in the studied Grashof numbers.

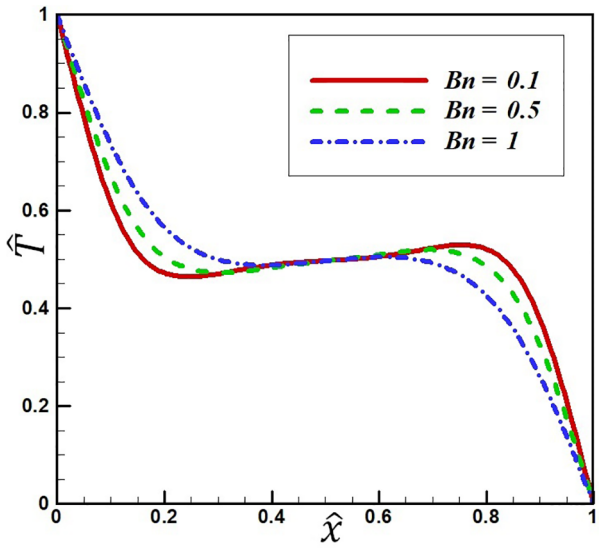

FIG. 18. The non-dimensional temperature in the middle of the cavity ($\hat{y} = 0.5$) for different Bingham numbers at $Gr = 10^4$ and $\phi_a = 0.04$.

V. CONCLUSION

The objective of this study was to introduce and develop an innovative Lattice Boltzmann method (LBM), which recovers the governing macroscopic equations of nanofluids for both single- and two-phase models, while it has the ability to deal with non-Newtonian behavior of nanofluids. The developed LBM has a different equilibrium density distribution function compared to the conventional Maxwell function, and it is a quadratic, which recovers all parts of the momentum equations directly, so it provides the opportunity to impose the desirable extra tensors and nanofluid thermophysical

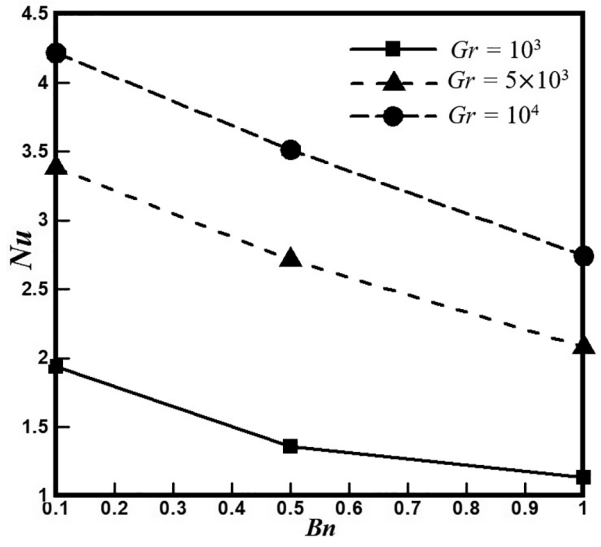

FIG. 19. The average Nusselt number for different Bingham and Grashof numbers at $\phi_a = 0.04$.

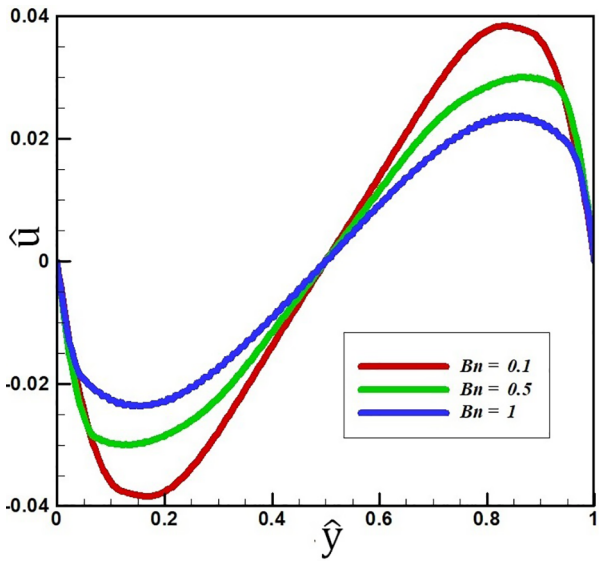

FIG. 20. The local non-dimensional horizontal velocity at $\hat{x} = 0.5$ for $Gr = 10^4$ and $\phi_a = 0.04$.

properties directly in this function. The same advantages are observed in the energy equation and the nanoconcentration equation for the two-phase model where we can apply the properties values in the parameters of the suggested equilibrium distribution functions easily. In contrast to common LBM, which is required to use specific relations for distribution functions, the boundary conditions are employed directly, so any types of boundaries including Neumann and Dirichlet ones can be utilized for the fluid flow, energy, and concentration parts simply, which makes the approach more convenient and practical than common LBMs. To have a continuous stability in this method, a

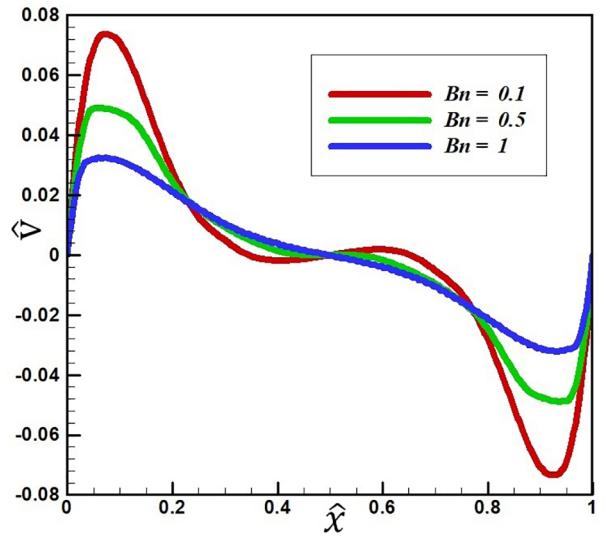

FIG. 21. The local non-dimensional vertical velocity at $\hat{y} = 0.5$ for $Gr = 10^4$ and $\phi_a = 0.04$.

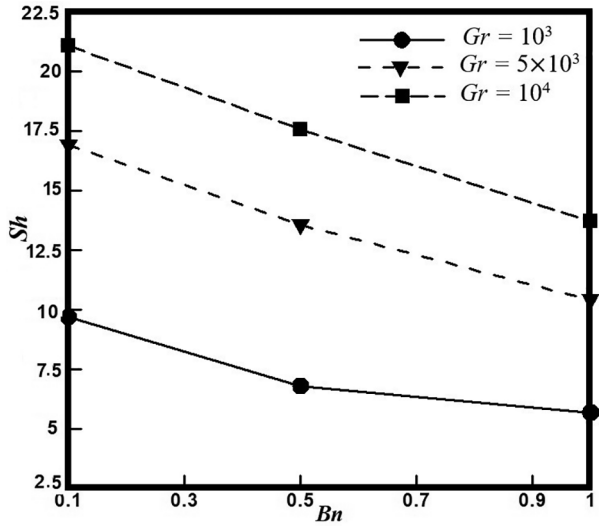

FIG. 22. The average Sherwood number for different Bingham and Grashof numbers at $\phi_a = 0.04$.

parameter is introduced, which can be altered based on the macroscopic the values and also satisfies the required CFL conditions regularly in the numerical marching and process. The common benchmark for studying the effect of different nanofluids, which has a Newtonian trend, on heat transfer in computational fluid dynamics (CFD) is natural convection in an enclosed cavity. The required dimensional and non-dimensional macroscopic and LBM equations for the single- and two-phase models were derived and presented in detail for the problem and the results illustrated a good agreement with previous CFD studies into Newtonian nanofluid for the selected benchmark problem. The experimental results from previous published studies demonstrated that some nanofluids with specific properties show non-Newtonian shear-thinning and Herschel–Bulkley (HB) behavior, so the models applied for the case of natural convection of nanofluids in a cavity based on the reported experimental results. It was observed that the average Nusselt number, which can be considered as an element for assessing the intensity of heat transfer process, declines by that the drop of power-law index in the power-law model of non-Newtonian nanofluid similar to pure fluids. The average Nusselt number ratio proved that the increase in Grashof number, which shows the ratio of the buoyancy to viscous force, enhances the effect of power-law index, so the effective parameters that can alter the Grashof number such as the temperature difference ΔT can change the influence of the power-law index. To apply the HB model, a traceless tensor is imposed to this model, which can distinguish the yield and unyielded zones clearly. In addition, there is no assumptions are employed for this approach. The two-phase model of nanofluid was used and the results of the introduced HB model based on the experimental data are reported. Interestingly, it was observed the maximum concentration of the nanoparticles is aggregated on the walls similar to the shown results of power-law fluids. In addition, symmetric unyielded/yielded zones are generated for the natural convection in the cavity like viscoplastic fluids in the absence of nanoparticles. In the experiment, results were reported that the increase in the volume

fraction of nanoparticle augments the yield stress (τ_y) and, as a result, the Bingham number, so the effect of Bingham number was evaluated on heat transfer and the outcomes were similar to regular viscoplastic fluids in the benchmark problem. In fact, the rise of Bingham number declines heat transfer gradually and the unyielded regions are expanded.

In future studies, the model will be developed for three-dimensional cases. In addition, the model has the potential to be considered for various velocities, thermal, and concentration boundary conditions, so it can be employed for any different cases and boundaries. Further, for curved boundaries, the method has the potential to be expanded with immersed boundary method, which was introduced[86] recently and makes the proposed method suitable for any complex curved boundaries. Further, the convection of Newtonian and non-Newtonian nanofluids through porous media with implementing the proposed method in our recent work.[87]

DATA AVAILABILITY

The data that support the findings of this study are available from the corresponding author upon reasonable request.

NOMENCLATURE

$\mathbf{A}$	First Rivlin–Ericksen tensor (1/s)
$\mathbf{a}$	Acceleration (m/s^2)
Bn	Bingham number
c	Nanofluid specific heat capacity (J/kg K)
D_B	Brownian diffusion coefficient (m^2/s)
D_T	Thermal diffusion coefficient (m^2/s)
d_p	Nanoparticle diameter (m)
$\mathbf{e}$	Discrete lattice velocity (m/s)
$\mathbf{e_y}$	Unit vector in y direction
F	Discrete body force (kg/m^3 s)
$\mathbf{f}$	External forces in the control volume (N/m^3)
f	Density distribution functions (kg/m^3)
f^{eq}	Equilibrium density distribution functions (kg/m^3)
G	Discrete source term in the energy distribution functions (W/m^3)
g	Internal energy distribution functions (J/m^3)
$\mathbf{g}$	Gravity acceleration (m/s^2)
g^{eq}	Equilibrium internal energy distribution functions (J/m^3)
Gr	Grashof number
h	Specific enthalpy (J/kg)
$\mathbf{j}$	Total nanoparticle mass flux (kg/m^2 s)
$\mathbf{j}_B$	Nanoparticle mass flux due to Brownian diffusion (kg/m^2 s)
$\mathbf{j}_T$	Nanoparticle mass flux to thermophoresis (kg/m^2 s)
K	Consistency factor of power-law model (Pa s^m)
k	Thermal conductivity (W/m K)
k_B	Boltzmann constant (J/K)
K_H	Consistency factor of Herschel–Bulkley model (Pa s^m)
Kn	Knudsen number
L	Length of the cavity (m)
Le	Lewis number
m	Power-law index
N_{BT}	Ratio of Brownian and thermophoretic diffusivities
Nu	Average Nusselt number
p	Pressure (Pa)
Pr	Prandtl number
$\mathbf{q}$	Total heat flux (W/m^2)
$\mathbf{q}_c$	Heat flux of conduction (W/m^2)
$\mathbf{q}_d$	Heat flux due to nanoparticle diffusion (W/m^2)
Ra	Rayleigh number
Re	Reynolds number
s_α	Concentration distribution functions of nanofluids (kg/m^3 s)
s_α^{eq}	Equilibrium concentration distribution functions of nanofluids (kg/m^3 s)
Sh	Sherwood number
T	Temperature (K)
t	Time (s)
x, y	Cartesian coordinates (m)
U	The buoyancy velocity scale (m/s)
u	Velocity in x direction (m/s)
v	Velocity in y direction (m/s)

Greek letters

β	Thermal expansion coefficient (1/K)
$\dot{\gamma}$	Shear rate (1/s)
Δt	Time increment (s)
Δx	Lattice spacing in x direction (m)
Δy	Lattice spacing in y direction (m)
ε	Small parameter for expansion
λ	Relaxation time (s)
μ	Dynamic viscosity (Pa s)
ρ	Density (kg/m^3)
$\boldsymbol{\tau}$	Extra stress tensor (Pa)
τ_y	Yield stress (Pa)
ϕ	Nanoparticle volume fraction
ϖ	Thermophoretic coefficient
$\mathbf{II}$	Viscoplasticity constraint tensor

Subscripts

C	Cold
f	Fluid
H	Hot
l	Local
n	Nanofluid
p	Nanoparticles
r	Reference
α	Direction α in a lattice

APPENDIX A: SELECTING APPROPRIATE Σ

We can write the distribution function in different directions by

$$f_0^{eq} = A_0, \quad f_1^{eq} = \frac{\rho_n}{2\sigma}u + \sigma^2\Lambda_{11}, \tag{A1}$$

$$f_5^{eq} = -\frac{\rho_n}{2\sigma}u + \sigma^2\Lambda_{11}, \tag{A2}$$

$$f_3^{eq} = \frac{\rho_n}{2\sigma}v + \sigma^2\Lambda_{22}, \quad f_7^{eq} = -\frac{\rho_n}{2\sigma}v + \sigma^2\Lambda_{22}, \tag{A3}$$

$$f_2^{eq} = f_6^{eq} = \Lambda_{12}, \quad f_4^{eq} = f_8^{eq} = -\Lambda_{12}. \tag{A4}$$

So, with multiplying the above relations of (A1)–(A4) by $|\mathbf{e}|^2/2$, we have

$$\sum_{\alpha=0}^{8}\frac{1}{2}f_\alpha^{eq}|\mathbf{e}_\alpha|^2 = p+\frac{1}{2}\rho_n|\mathbf{u}|^2-\frac{\tau_{xx}+\tau_{yy}}{2}, \tag{A5}$$

with the relation for the force term in the text, we can show

$$\sum_{\alpha=0}^{8}F_\alpha|\mathbf{e}_\alpha|^2 = 0. \tag{A6}$$

In addition, the streaming part of the Lattice Boltzmann equation (LBE) and the initial value of f_α is substituted with f_α^{eq} and is written as

$$\frac{\partial f_\alpha^{eq}}{\partial t}+\mathbf{e}_\alpha\cdot\nabla_{\mathbf{x}}f_\alpha^{eq}-F_\alpha = 0, \tag{A7}$$

with the importing the above relations in (A7)

$$\frac{\partial}{\partial t}\left[p+\frac{1}{2}\rho_n|\mathbf{u}|^2-\frac{\tau_{xx}+\tau_{yy}}{2}\right]+\frac{\sigma^2}{2}(\rho_n(\nabla\cdot\mathbf{u})) = O(\varepsilon). \tag{A8}$$

The Courant–Friedrichs–Lewy (CFL) condition gives

$$\Upsilon = \frac{u\Delta t}{\Delta x}+\frac{v\Delta t}{\Delta y}\le 1, \tag{A9}$$

the incompressibility and unique pressure generates $\tau_{xx}+\tau_{yy}=0$. Consequently, (A8) is defined by

$$\left[|\mathbf{u}|^2+\frac{2p}{\rho_n}\right]+\sigma^2\Upsilon = O(\varepsilon). \tag{A10}$$

Thus,

$$\sigma = \frac{1}{\sqrt{\Upsilon}}\sqrt{\left|\frac{-2p}{\rho_n}-|\mathbf{u}|^2\right|}. \tag{A11}$$

APPENDIX B: THE LBM FOR RECOVERING THE MOMENTUM EQUATION

The basic equation of the single particle distribution function $[f=f(\mathbf{x},\mathbf{e},t)]$ is presented by $\frac{Df}{Dt}=Q(f)$, and we have

$$\frac{Df}{Dt} = \frac{\partial f}{\partial \mathbf{x}}\frac{D\mathbf{x}}{Dt}+\frac{\partial f}{\partial \mathbf{e}}\frac{D\mathbf{e}}{Dt}+\frac{\partial f}{\partial t}\frac{Dt}{Dt}, \tag{B1}$$

where

$$\frac{D\mathbf{x}}{Dt}=\mathbf{e}, \quad \frac{D\mathbf{e}}{Dt}=\mathbf{a}. \tag{B2}$$

Here, $\mathbf{e}$ is velocity at position $\mathbf{x}$ and time t for particles and $\mathbf{a}$ is the particles acceleration. $Q(f)$ is the collision operator, which satisfies the governing macroscopic equations, including the mass, momentum, and energy conservation. The Bhatnagar–Gross–Krook (BGK) collision approximation is usually applied for the collision part and calculated as

$$Q(f) = \frac{1}{\lambda}(f-f^{eq}), \tag{B3}$$

where λ is the collision relaxation time, and f_α^{eq} is the equilibrium lattice function. The discretized non-dimensional form of LBE with applying the BGK model can be written as

$$\frac{\partial f_\alpha}{\partial t}+\mathbf{e}_\alpha\cdot\nabla_{\mathbf{x}}f_\alpha+\mathbf{a}\cdot\nabla_{\mathbf{e}}f_\alpha = -\frac{1}{\varepsilon\,\lambda_f}(f_\alpha-f_\alpha^{eq}). \tag{B4}$$

The parameter ε is a small parameter, which plays the role of the Knudsen number (Kn) for considering the order of terms and quantities in the equations. λ_f is the non-dimensional relaxation time ($\lambda_f=\lambda/\Delta t$). The third term of (B4), which contains the acceleration for a unit mass, is defined as

$$\mathbf{a}\cdot\nabla_{\mathbf{e}}f_\alpha \approx -F_\alpha. \tag{B5}$$

The conditions, which should be applied for the force term (F_α) in D2Q9, are

$$\sum_{\alpha=0}^{8}F_\alpha = 0, \quad \sum_{\alpha=0}^{8}F_\alpha\mathbf{e}_\alpha = \mathbf{f}. \tag{B6}$$

So, (B4) is modified as

$$\frac{\partial f_\alpha}{\partial t}+\mathbf{e}_\alpha\cdot\nabla_{\mathbf{x}}f_\alpha-F_\alpha = -\frac{1}{\varepsilon\,\lambda_f}(f_\alpha-f_\alpha^{eq}). \tag{B7}$$

In this approach, we apply basic assumptions and relation between f_α^{eq} and the macroscopic parameters to satisfy the mass and momentum equations. For a two-dimensional case with applying the D2Q9, the mentioned conditions are

$$\sum_{\alpha=0}^{8}f_\alpha^{eq} = \rho_n, \quad \sum_{\alpha=0}^{8}f_\alpha^{eq}\mathbf{e}_\alpha = \rho_n\,\mathbf{u}, \tag{B8}$$

$$\sum_{\alpha=0}^{8}f_\alpha^{eq}\mathbf{e}_\alpha\otimes\mathbf{e}_\alpha = \mathbf{M}_2, \tag{B9}$$

$$\sum_{\alpha=0}^{8}f_\alpha^{(a)} = 0,\ a\ge 1; \quad \sum_{\alpha=0}^{8}f_\alpha^{(a)}\mathbf{e}_\alpha = 0,\ a\ge 1. \tag{B10}$$

The matrix $\mathbf{M}_2$ is defined by

$$\mathbf{M}_2 = \begin{bmatrix}\rho_n u^2+p-\tau_{xx} & \rho_n uv-\tau_{xy}\\ \rho_n uv-\tau_{xy} & \rho_n v^2+p-\tau_{yy}\end{bmatrix}. \tag{B11}$$

A Chapman–Enskog type expansion for f_α has the following expansion:

$$f_\alpha = f_\alpha^{eq}+\varepsilon f_\alpha^{(1)}+\varepsilon^2 f_\alpha^{(2)}+O(\varepsilon^3), \tag{B12}$$

if we substitute Eq. (B12) in Eq. (B7) and sum the resultant equation, we have

$$\frac{\partial}{\partial t}\left(\sum_{\alpha=0}^{8}f_\alpha^{eq}\right)+\nabla\cdot\left(\sum_{\alpha=0}^{8}f_\alpha^{eq}\mathbf{e}_\alpha\right)-\sum_{\alpha=0}^{8}F_\alpha = -\sum_{\alpha=0}^{8}\frac{1}{\lambda_f}f_\alpha^{(1)}+O(\varepsilon), \tag{B13}$$

since we are considering the incompressible flow ($\rho_n = constant$) and applying the mentioned relations in (B8)–(B10), it results in the continuity equation as

$$\rho_n(\nabla.\mathbf{u}) = 0 + O(\varepsilon). \tag{B14}$$

If we multiply Eq. (B7) by $\mathbf{e}_\alpha$ and sum over it, we have

$$\frac{\partial}{\partial t}\left(\sum_{\alpha=0}^{8} f_\alpha^{eq}\mathbf{e}_\alpha\right) + \sum_{\alpha=0}^{8}\left(\mathbf{e}_\alpha \cdot \left(\nabla f_\alpha^{eq} \cdot \mathbf{e}_\alpha\right)\right) - \sum_{\alpha=0}^{8} F_\alpha \mathbf{e}_\alpha = -\sum_{\alpha=0}^{8}\frac{1}{\lambda_f} f_\alpha^{(1)}\mathbf{e}_\alpha + O(\varepsilon), \tag{B15}$$

where

$$\mathbf{e}_\alpha \cdot \left(\nabla f_\alpha^{eq} \cdot \mathbf{e}_\alpha\right) = \nabla \cdot \left(f_\alpha^{eq}\mathbf{e}_\alpha \otimes \mathbf{e}_\alpha\right), \tag{B16}$$

with considering the cited conditions in (B7)–(B12), one obtains

$$\rho_n \frac{\partial \mathbf{u}}{\partial t} + \nabla \cdot \mathbf{M}_2 - \mathbf{f} = \mathbf{0} + O(\varepsilon), \tag{B17}$$

with substituting the parameters of $\mathbf{M}_2$ in (B17), the momentum equation is given by

$$\rho_n\left[\frac{\partial \mathbf{u}}{\partial t} + (\mathbf{u}.\nabla)\mathbf{u}\right] + \nabla p - \nabla \cdot \boldsymbol{\tau} - \mathbf{F} = \mathbf{0} + O(\varepsilon), \tag{B18}$$

where (B18) shows the LBM equations recover the momentum equation.

APPENDIX C: THE LBM FOR RECOVERING THE ENERGY EQUATION

1. Two-phase model

The energy distribution function g_α is written as

$$\frac{\partial g_\alpha}{\partial t} + \mathbf{e}_\alpha \cdot \nabla_{\mathbf{x}} g_\alpha - G_\alpha = -\frac{1}{\varepsilon\lambda_g}(g_\alpha - g_\alpha^{eq}). \tag{C1}$$

The conditions of g_α and the equilibrium energy distribution function g_α^{eq}, which should be applied to satisfy the energy equation, are

$$\sum_{\alpha=0}^{8} g_\alpha^{(n)} = 0, \quad n \geq 1, \quad \sum_{\alpha=0}^{8} g_\alpha^{eq} = (\rho c)_n T, \tag{C2}$$

$$\sum_{\alpha=0}^{8} g_\alpha^{eq}\mathbf{e}_\alpha = (\rho c)_n T\mathbf{u} + \mathbf{q}, \tag{C3}$$

$$\sum_{\alpha=0}^{8} G_\alpha = -h_p \nabla \cdot \mathbf{j}. \tag{C4}$$

If the g_α is expended by the Chapman–Enskog expression as

$$g_\alpha = g_\alpha^{eq} + \varepsilon g_\alpha^{(1)} + \varepsilon^2 g_\alpha^{(2)} + O(\varepsilon^3). \tag{C5}$$

With substitution of Eq. (C5) in (C1), we have

$$\frac{\partial}{\partial t}\left(\sum_{\alpha=0}^{8} g_\alpha^{eq}\right) + \nabla \cdot \left(\sum_{\alpha=0}^{8} g_\alpha^{eq}\mathbf{e}_\alpha\right) - \sum_{\alpha=0}^{8} G_\alpha = -\sum_{\alpha=0}^{8}\frac{1}{\lambda_g} g_\alpha^{(1)} + O(\varepsilon). \tag{C6}$$

Considering the mentioned conditions in (C2)–(C4) and applying through (C6), one finds that

$$\frac{\partial}{\partial t}\left((\rho c)_n T\right) + \nabla\left((\rho c)_n T\mathbf{u} + \mathbf{q}\right) + h_p \nabla \cdot \mathbf{j} = \mathbf{0} + O(\varepsilon), \tag{C7}$$

where

$$\nabla \cdot (T\mathbf{u}) = T \cdot (\nabla \cdot \mathbf{u}) + \mathbf{u} \cdot (\nabla T) \equiv \mathbf{u} \cdot \nabla T \tag{C8}$$

and

$$\nabla \cdot (h_p \mathbf{j}) = h_p \cdot (\nabla \cdot \mathbf{j}) + \mathbf{j} \cdot (\nabla h_p). \tag{C9}$$

Thus,

$$(\rho c)_n\left[\frac{\partial T}{\partial t} + \mathbf{u} \cdot \nabla T\right] + \nabla \cdot \mathbf{q} - h_p \nabla \cdot \mathbf{j} = \mathbf{0} + O(\varepsilon). \tag{C10}$$

2. Single-phase model

In the single-phase model, the energy distribution function equations in (C1) and the applied relation in (C2) are the same. The (C3) and (C4) are modified as

$$\sum_{\alpha=0}^{8} g_\alpha^{eq}\mathbf{e}_\alpha = (\rho c)_n T\mathbf{u} + \mathbf{q}_c, \tag{C11}$$

$$\sum_{\alpha=0}^{8} G_\alpha = 0, \tag{C12}$$

with using the Chapman–Enskog expression in (C5) and applying the updated conditions in (C6), (C7) is changed as

$$\frac{\partial}{\partial t}\left((\rho c)_n T\right) + \nabla\left((\rho c)_n T\mathbf{u} + \mathbf{q}_c\right) = \mathbf{0} + O(\varepsilon), \tag{C13}$$

with considering (C8)–(C9), we find that

$$(\rho c)_n\left[\frac{\partial T}{\partial t} + \mathbf{u} \cdot \nabla T\right] + \nabla \cdot \mathbf{q}_c = \mathbf{0} + O(\varepsilon). \tag{C14}$$

Hence, (C14) represents the energy equation for the single-phase model.

APPENDIX D: THE LBM FOR RECOVERING THE NANOPARTICLE EQUATION IN THE TWO-PHASE MODEL

The nanoparticle distribution function s_α is

$$\frac{\partial s_\alpha}{\partial t} + \mathbf{e}_\alpha \cdot \nabla_{\mathbf{x}} s_\alpha = -\frac{1}{\varepsilon\lambda_s}(s_\alpha - s_\alpha^{eq}). \tag{D1}$$

The introduced equilibrium nanoparticle distribution function s_α^{eq} is defined as

$$\sum_{\alpha=0}^{8} s_\alpha^{(n)} = 0, \quad n \geq 1, \quad \sum_{\alpha=0}^{8} s_\alpha^{eq} = \rho_p \phi, \tag{D2}$$

$$\sum_{\alpha=0}^{8} s_\alpha^{eq}\mathbf{e}_\alpha = \rho_p \phi\mathbf{u} + \mathbf{j}, \tag{D3}$$

with the Chapman–Enskog expression, the s_α is defined as

$$s_\alpha = s_\alpha^{eq} + \varepsilon s_\alpha^{(1)} + \varepsilon^2 s_\alpha^{(2)} + O(\varepsilon^3)\,. \tag{D4}$$

Applying Eq. (D4) in (D1) and summing them over the particles, we have

$$\frac{\partial}{\partial t}\left(\sum_{\alpha=0}^{8} s_\alpha^{eq}\right) + \nabla\cdot\left(\sum_{\alpha=0}^{8} s_\alpha^{eq}\mathbf{e}_\alpha\right) = -\sum_{\alpha=0}^{8}\frac{1}{\lambda_s} s_\alpha^{(1)} + O(\varepsilon), \tag{D5}$$

using (D2) and (D3) in (D5), one finds that

$$\frac{\partial}{\partial t}\left(\rho_p\phi\right) + \nabla\cdot\left(\rho_p\phi\mathbf{u} + \mathbf{j}\right) = \mathbf{0} + O(\varepsilon), \tag{D6}$$

where

$$\nabla\cdot(\phi\mathbf{u}) = \phi\cdot(\nabla\cdot\mathbf{u}) + \mathbf{u}\cdot(\nabla\phi) \equiv \mathbf{u}\cdot\nabla\phi, \tag{D7}$$

so,

$$\rho_p\left[\frac{\partial\phi}{\partial t} + \mathbf{u}\cdot\nabla\phi\right] + \nabla\cdot\mathbf{j} = \mathbf{0} + O(\varepsilon). \tag{D8}$$

Here, (D8) shows the equation of nanoparticles.

APPENDIX E: THE VISCOPLASTICITY CONSTRAINT TENSOR

The symmetric traceless tensor $\mathbf{II}$ has the following conditions:

$$\mathbf{1}:\mathbf{II} = 0, \tag{E1a}$$

$$\mathbf{II}:\mathbf{II} < 1, \quad \mathbf{A} = \mathbf{0}, \tag{E1b}$$

$$\mathbf{II}:\mathbf{II} = 1, \quad \mathbf{A} \neq \mathbf{0}. \tag{E1c}$$

The above presented conditions provide the required relation for the stress tensor of viscoplastic fluids, viz., $|\boldsymbol{\tau}| \le \tau_y$ at $\mathbf{A} = \mathbf{0}$, and $\tau_y < |\boldsymbol{\tau}|$ for $\mathbf{A} \neq \mathbf{0}$. The unyielded part (or the rigid section) and the yielded section (or the liquid part) are defined through the tensor $\mathbf{II}$ with satisfying Eq. (5) and applying the following steps and process:

- The introduced relations in Eq. (5) are imposed over the entire flow domain (including both yielded and unyielded sections).
- Finding the solutions of velocity $\mathbf{u}$ and the viscoplasticity constraint tensor $\mathbf{II}$ to reveal the yielded/unyielded regions. There are no singularities due to $\mathbf{A}/\dot{\gamma}$ as $\mathbf{A} \to \mathbf{0}$.
- The two unknown vectors of $\mathbf{u}$ and $\mathbf{II}$ should be defined, which requires a connection between these two vectors. It is proved that there is a relation between them using a simple projection operation $(PR_{\mathcal{M}})$[72,76–78] as

$$\mathbf{II} = PR_{\mathcal{M}}(\mathbf{II} + r\tau_y\mathbf{A}), \quad \forall r > 0, \tag{E2}$$

where

$$\mathcal{M} = \left\{\boldsymbol{\chi}|\boldsymbol{\chi} = (\chi_{ij})_{1\le i,j\le 2} \in (L^2(\Omega))^4, \|\boldsymbol{\chi}\| \le 1 \text{ a.e. on } \Omega\right\} \quad \text{and} \quad PR_{\mathcal{M}} : (L^2(\Omega))^4 \to \mathcal{M}, \tag{E3}$$

is the projection operator defined so that $PR_{\mathcal{M}}(\boldsymbol{\chi}) = \boldsymbol{\chi}$, if $\|\boldsymbol{\chi}\| \le 1$, and $P_{\mathcal{M}}(\boldsymbol{\chi}) = \boldsymbol{\chi}/\|\boldsymbol{\chi}\|$ otherwise. Note that in the context of Eq. (2), the tensor $\boldsymbol{\chi} = \mathbf{II} + r\tau_y\mathbf{A}$ and it is symmetric. Further, the tensor $\boldsymbol{\chi}$ must be dimensionless for $\mathbf{II}$ is also dimensionless.

Here, $r > 0$ is a value, which can be defined by non-dimensional parameters based on our studied case and problem. The iterations will continue to reach the convergence point based on our desired accuracy. It should be noted that the boundary between the yielded and unyielded regions is shaped between $||\mathbf{II}|| < 1$ and $||\mathbf{II}|| = 1$.

REFERENCES

[1] S. U. S. Choi and J. Eastman, "Enhancing thermal conductivity of fluids with nanoparticles," in ASME International Mechanical Engineering Congress & Exposition, 1995.
[2] S. Kumar Das, S. U. S. Choi, and H. E. Patel, "Heat transfer in nanofluids—A review," Heat Transfer Eng. **27**, 3–19 (2006).
[3] L. Qiu, N. Zhu, Y. Feng, E. E. Michaelides, G. Zyia, D. Jing, X. Zhang, P. M. Norris, C. N. Markides, and O. Mahian, "A review of recent advances in thermophysical properties at the nanoscale: From solid state to colloids," Phys. Rep. **843**, 1–81 (2020).
[4] K. Bashirnezhad, S. Bazri, M. R. Safaei, M. Goodarzi, M. Dahari, O. Mahian, A. S. Dalkiliça, and S. Wongwises, "Viscosity of nanofluids: A review of recent experimental studies," Int. Commun. Heat Mass Transfer **73**, 114 (2016).
[5] R. Saidura, K. Y. Leong, and H. A. Mohammad, "A review on applications and challenges of nanofluids," Renewable Sustainable Energy Rev. **15**, 1646 (2011).
[6] S. M. Vanaki, P. Ganesan, and H. A. Mohammed, "Numerical study of convective heat transfer of nanofluids: A review," Renewable Sustainable Energy Rev. **54**, 1212 (2016).
[7] K. Khanafer, K. Vafai, and M. Lightstone, "Buoyancy-driven heat transfer enhancement in a two-dimensional enclosure utilizing nanofluids," Int. J. Heat Mass Transfer **46**, 3639 (2003).
[8] R. Jou and S. Tzeng, "Numerical research of nature convective heat transfer enhancement filled with nanofluids in rectangular enclosures," Int. Commun. Heat Mass Transfer **33**, 727 (2006).
[9] H. F. Oztop and E. Abu-Nada, "Numerical study of natural convection in partially heated rectangular enclosures filled with nanofluids," Int. J. Heat Fluid Flow **29**, 1326 (2008).
[10] M. M. Rashidi, M. Sadri, and M. A. Sheremet, "Numerical simulation of hybrid nanofluid mixed convection in a lid-driven square cavity with magnetic field using high-order compact scheme," Nanomaterials **11**, 2250 (2021).
[11] Y. Ma, R. Mohebbi, M. M. Rashidi, and Z. Yang, "Numerical study of MHD nanofluid natural convection in a baffled U-shaped enclosure," Int. J. Heat Mass Transfer **130**, 123 (2019).
[12] M. M. Rashidi, M. Nasiri, M. Khezerloo, and N. Laraqi, "Numerical investigation of magnetic field effect on mixed convection heat transfer of nanofluid in a channel with sinusoidal walls," J. Magn. Magn. Mater. **401**, 159 (2016).
[13] Y. Ding, H. Alias, D. sheng, W. Richard, and A. Williams, "Heat transfer of aqueous suspensions of carbon nanotubes (CNT nanofluids)," Int. J. Heat Mass Transfer **49**, 240 (2006).
[14] B. Aladag, S. Halelfadl, N. Doner, T. Maré, S. Duret, and P. Estellé, "Experimental investigations of the viscosity of nanofluids at low temperatures," Appl. Energy **97**, 876 (2012).
[15] A. Ouahouah, N. Labsi, X. Chesneau, and Y. Benkahla, "Natural convection within a non-uniformly heated cavity partly filled with a shear-thinning nanofluid and partly with air," J. Non-Newtonian Fluid Mech. **289**, 104490 (2021).
[16] A. V. Minakov, V. Y. Rudyak, and M. I. Pryazhnikov, "Rheological behavior of water and ethylene glycol based nanofluids containing oxide nanoparticles," Colloids Surf. A **554**, 279 (2018).
[17] S. Ouyahia, Y. Benkahla, W. Berabou, and A. Boudiaf, "Numerical study of the flow in a square cavity filled with carbopol-TiO_2 nanofluid," Powder Technol. **311**, 101 (2017).
[18] S. Lahlou, N. Labsi, Y. K. Benkahla, A. Boudiaf, and S. Ouyahia, "Flow of viscoplastic fluids containing hybrid nanoparticles: Extended Buongiorno's model," J. Non-Newtonian Fluid Mech. **281**, 104308 (2020).
[19] J. Buongiorno, "Convective transport in nanofluids," J. Heat Transfer **128**, 240 (2006).
[20] D. Y. Tzou, "Instability of nanofluids in natural convection," ASME J. Heat Transfer **130**, 072401 (2008).

[21]D. Y. Tzou, "Thermal instability of nanofluids in natural convection," Int. J. Heat Mass Transfer **51**, 2967 (2008).
[22]M. Corcione, M. Cianfrini, and A. Quintino, "Two-phase mixture modeling of natural convection of nanofluids with temperature-dependent properties," Int. J. Therm. Sci. **71**, 182 (2013).
[23]D. A. Nield and A. V. Kuznetsov, "The onset of convection in a horizontal nanofluid layer of finite depth," Eur. J. Mech.-B **29**, 217 (2010).
[24]D. A. Nield and A. V. Kuznetsov, "The onset of convection in a horizontal nanofluid layer of finite depth: A revised model," Int. J. Heat Mass Transfer **77**, 915 (2014).
[25]Z. Haddad, E. Abu-Nada, H. F. Oztop, and A. Mataoui, "Natural convection in nanofluids: Are the thermophoresis and Brownian motion effects significant in nanofluid heat transfer enhancement?," Int. J. Therm. Sci. **57**, 152 (2012).
[26]D. A. Nield and A. V. Kuznetsov, "The Cheng–Minkowycz problem for natural convective boundary layer flow in a porous medium saturated by a nanofluid," Int. J. Heat Mass Transfer **52**, 5792 (2009).
[27]D. A. Nield and A. V. Kuznetsov, "Thermal instability in a porous medium layer saturated by a nanofluid," Int. J. Heat Mass Transfer **52**, 5796 (2009).
[28]M. A. Sheremet, I. Pop, and M. M. Rahman, "Three-dimensional natural convection in a porous enclosure filled with a nanofluid using Buongiorno's mathematical model," Int. J. Heat Mass Transfer **82**, 396 (2015).
[29]J. Kang, F. Zhou, W. Tan, and T. Xia, "Thermal instability of non-homogeneous power-law nanofluid in a porous layer with horizontal through," J. Non-Newtonian Fluid Mech. **213**, 50–56 (2014).
[30]S. Chen and G. D. Doolen, "Lattice Boltzmann method for fluid flows," Annu. Rev. Fluid Mech. **30**, 329 (1998).
[31]S. Succi, *The Lattice Boltzmann Equation: For Fluid Dynamics and Beyond* (Oxford University Press, 2001).
[32]A. A. Mohamad, *Lattice Boltzmann Method: Fundamentals and Engineering Applications with Computer Codes* (Springer, 2011).
[33]Z. Guo, B. Shi, and N. Wang, "Lattice BGK model for incompressible Navier-Stokes equation," J. Comput. Phys. **165**, 288–306 (2000).
[34]Z. Chen, C. Shu, L. M. Yang, X. Zhao, and N. Y. Liu, "Immersed boundary-simplified thermal lattice Boltzmann method for incompressible thermal flows," Phys. Fluids **32**, 013605 (2020).
[35]O. Ilyin, "Gaussian Lattice Boltzmann method and its applications to rarefied flows," Phys. Fluids **32**, 012007 (2020).
[36]Q. Li, Z. Lu, D. Zhou, X. Niu, T. Guo, and B. Du, "Unified simplified multiphase lattice Boltzmann method for ferrofluid flows and its application," Phys. Fluids **32**, 093302 (2020).
[37]Y. Zong, C. Zhang, H. Liang, L. Wang, and J. Xu, "Modeling surfactant-laden droplet dynamics by lattice Boltzmann method," Phys. Fluids **32**, 122105 (2020).
[38]G. Farag, S. Zhao, T. Coratger, P. Boivin, G. Chiavassa, and P. Sagaut, "A pressure-based regularized lattice-Boltzmann method for the simulation of compressible flows," Phys. Fluids **32**, 066106 (2020).
[39]L. Xu, X. Yu, and K. Regenauer-Lieb, "An immersed boundary-lattice Boltzmann method for gaseous slip flow," Phys. Fluids **32**, 012002 (2020).
[40]Y. Xuan and Z. Yao, "Lattice Boltzmann model for nanofluids," Heat Mass Transfer **41**, 199 (2004).
[41]G. H. R. Kefayati, S. F. Hosseinizadeh, M. Gorji, and H. Sajjadi, "Lattice Boltzmann simulation of natural convection in tall enclosures using water/SiO_2 nanofluid," Int. Commun. Heat Mass Transfer **38**, 798 (2011).
[42]H. Nemati, M. Farhadi, K. Sedighi, E. Fattahi, and A. A. R. Darzi, "Lattice Boltzmann simulation of nanofluid in lid-driven cavity," Int. Commun. Heat Mass Transfer **37**, 1528 (2010).
[43]H. Sajjadi, M. Gorji, G. H. R. Kefayati, and D. D. Ganji, "Lattice Boltzmann simulation of turbulent natural convection in tall enclosures using Cu/Water nanofluid," Numer. Heat Transfer, Part A **62**, 512 (2012).
[44]E. Fattahi, M. Farhadi, K. Sedighi, and H. Nemati, "Lattice Boltzmann simulation of natural convection heat transfer in nanofluids," Int. J. Therm. Sci. **52**, 137 (2012).
[45]W. N. Zhou, Y. Y. Yan, and J. L. Xu, "A lattice Boltzmann simulation of enhanced heat transfer of nanofluids," Int. Commun. Heat Mass Transfer **55**, 113 (2014).
[46]N. A. Che Sidik and R. Mamat, "Recent progress on lattice Boltzmann simulation of nanofluids: A review," Int. Commun. Heat Mass Transfer **66**, 11–22 (2015).
[47]H. Sajjadi, A. A. Delouie, M. Atashafrooz, and M. Sheikholeslami, "Double MRT lattice Boltzmann simulation of 3-D MHD natural convection in a cubic cavity with sinusoidal temperature distribution utilizing nanofluid," Int. J. Heat Mass Transfer **126**, 489 (2018).
[48]O. Aliu, H. Sakidin, J. Foroozesh, and N. Yahya, "Lattice Boltzmann application to nanofluids dynamics—A review," J. Mol. Liq. **300**, 112284 (2020).
[49]Y. Ma and Z. Yang, "Simplified and highly stable thermal Lattice Boltzmann method simulation of hybrid nanofluid thermal convection at high Rayleigh numbers," Phys. Fluids **32**, 012009 (2020).
[50]R. Mohebbi, M. Izadi, and A. J. Chamkha, "Heat source location and natural convection in a C-shaped enclosure saturated by a nanofluid," Phys. Fluids **29**, 122009 (2017).
[51]Y. Ma, R. Mohebbi, M. M. Rashidi, and Z. Yang, "Study of nanofluid forced convection heat transfer in a bent channel by means of lattice Boltzmann method," Phys. Fluids **30**, 032001 (2018).
[52]A. A. Mehrizi, F. Besharati, O. Jahanian, and H. Hassanzadeh Afrouzi, "Numerical investigation of conjugate heat transfer in a microchannel with a hydrophobic surface utilizing nanofluids under a magnetic field," Phys. Fluids **33**, 052002 (2021).
[53]R. Soleimani, M. Zargartalebi, J. Azaiez, and I. D. Gates, "Hydrodynamic analysis of nanofluid's convective heat transfer in channels with extended surfaces," Phys. Fluids **33**, 012011 (2021).
[54]M. Zargartalebi and J. Azaiez, "Mesoscopic study of miscible nanoflow instabilities," Phys. Fluids **30**, 024105 (2018).
[55]S. C. Fu, W. W. F. Leung, and R. M. C. So, "A lattice Boltzmann method based numerical scheme for microchannel Flows," J. Fluids Eng. **131**, 081401 (2009).
[56]S. C. Fu and R. M. C. So, "Modeled lattice Boltzmann equation and the constant-density assumption," AIAA J. **47**, 3038–3042 (2009).
[57]S. C. Fu, R. M. C. So, and R. M. C. Leung, "Linearized-Boltzmann-type-equation-based finite difference method for thermal incompressible flow," Comput. Fluids **69**, 67–80 (2012).
[58]R. R. Huilgol and G. H. R. Kefayati, "From mesoscopic models to continuum mechanics: Newtonian and non-Newtonian fluids," J. Non-Newtonian Fluid Mech. **233**, 146–154 (2016).
[59]P. D. Lax and B. Wendroff, "Systems of conservation laws," Commun. Pure Appl. Math. **13**, 217 (1960).
[60]L. Sundar, E. Ramana, M. Singh, and A. D. Sousa, "Viscosity of low volume concentrations of magnetic Fe_3O_4 nanoparticles dispersed in ethylene glycol and water mixture," Chem. Phys. Lett. **554**, 236 (2012).
[61]T. Phuoc, M. Massoudi, and R. Chen, "Viscosity and thermal conductivity of nanofluids containing multi-walled carbon nanotubes stabilized by chitosan," Int. J. Therm. Sci. **50**, 12–18 (2011).
[62]P. Garg, J. Alvarado, C. Marsh, T. Carlson, D. Kessler, and K. Annamalai, "An experimental study on the effect of ultrasonication on viscosity and heat transfer performance of multi-wall carbon nanotube-based aqueous nanofluids," Int. J. Heat Mass Transfer **52**, 5090 (2009).
[63]L. Maillaud, P. Poulin, M. Pasquali, and C. Zakri, "Effect of the rheological properties of carbon nanotube dispersions on the processing and properties of transparent conductive electrodes," Langmuir **31**, 5928 (2015).
[64]C. Nguyen, F. Desgranges, N. Galanis, G. Roy, T. Maré, S. Boucher *et al.*, "Viscosity data for Al_2O_3-water nanofluid-hysteresis: Is heat transfer enhancement using nanofluids reliable?," Int. J. Therm. Sci. **47**, 103 (2008).
[65]C. T. Nguyena, F. Desgranges, G. Roy, N. Galanis, T. Maré, S. Boucher, and H. A. Mintsa, "Temperature and particle-size dependent viscosity data for water-based nanofluids—hysteresis phenomenon," Int. J. Heat Fluid Flow **28**, 1492 (2007).
[66]G. B. Kim, J. M. Hyun, and H. S. Kwak, "Transient buoyant convection of a power-law non-Newtonian fluid in an enclosure," Int. J. Heat Mass Transfer **46**, 3605 (2003).
[67]O. Turan, A. Sachdeva, R. J. Poole, and N. Chakraborty, "Laminar natural convection of power-law fluids in a square enclosure with differentially heated sidewalls subjected to constant wall heat flux," J. Heat Transfer **134**, 122504 (2012).
[68]O. Turan, A. Sachdeva, N. Chakraborty, and R. J. Poole, "Laminar natural convection of power-law fluids in a square enclosure with differentially heated side walls subjected to constant Temperatures," J. Non-Newtonian Fluid Mech. **166**, 1049–1063 (2011).

[69]L. Khezzar, D. Siginer, and I. Vinogradov, "Natural convection of power law fluids in inclined cavities," Int. J. Therm. Sci. **53**, 8–17 (2012).
[70]C. Sasmal, A. K. Gupta, and R. P. Chhabra, "Natural convection heat transfer in a power-law fluid from a heated rotating cylinder in a square duct," Int. J. Heat Mass Transfer **129**, 975–996 (2019).
[71]A. K. Tiwari and R. P. Chhabra, "Laminar natural convection in power-law liquids from a heated semi-circular cylinder with its flat side oriented downward," Int. J. Heat Mass Transfer **58**, 553–567 (2013).
[72]R. R. Huilgol, *Fluid Mechanics of Viscoplasticity* (Springer, 2015).
[73]D. Cabaleiro, M. J. Pastoriza-Gallego, C. Gracia-Fernández, M. M. Piñeiro, and L. Lugo, "Rheological and volumetric properties of TiO_2-ethylene glycol nanofluids," Nanoscale Res. Lett. **8**, 286 (2013).
[74]R. Shu, Y. Gun, H. Lv, and D. Tan, "Preparation and rheological behavior of ethylene glycol-based TiO_2 nanofluids," Colloids Surf., A **509**, 86 (2016).
[75]G. Zyla, J. P. Vallejo, J. Fal, and L. Lugu, "Nanodiamonds—Ethylene glycol nanofluids: Experimental investigation of fundamental physical properties," Int. J. Heat Mass Transfer **121**, 1201 (2018).
[76]R. R. Huilgol and G. H. R. Kefayati, "Natural convection problem in a Bingham fluid using the operator-splitting method," J. Non-Newtonian Fluid Mech. **220**, 22 (2015).
[77]G. H. R. Kefayati and R. R. Huilgol, "Lattice Boltzmann Method for simulation of mixed convection of a Bingham fluid in a lid-driven cavity," Int. J. Heat Mass Transfer **103**, 725 (2016).
[78]R. R. Huilgol and G. H. R. Kefayati, "A particle distribution function approach to the equations of continuum mechanics in Cartesian, cylindrical and spherical coordinates: Newtonian and non-Newtonian fluids," J. Non-Newtonian Fluid Mech. **251**, 119 (2018).
[79]O. Turan, N. Chakraborty, and R. J. Poole, "Laminar natural convection of Bingham fluids in a square enclosure with differentially heated side walls," J. Non-Newtonian Fluid Mech. **165**, 901 (2010).
[80]G. R. Kefayati, "Lattice Boltzmann simulation of double diffusive natural convection of viscoplastic fluids in a porous cavity," Phys. Fluids **31**, 013105 (2019).
[81]G. R. Kefayati, H. Tang, and A. Chan, "Immersed boundary-finite difference lattice Boltzmann method through fluid-structure interaction for viscoplastic fluids," J. Fluids Struct. **83**, 238 (2018).
[82]G. R. Kefayati and H. Tang, "MHD mixed convection of viscoplastic fluids in different aspect ratios of a lid-driven cavity using LBM," Int. J. Heat Mass Transfer **124**, 344 (2018).
[83]G. R. Kefayati and H. Tang, "Lattice Boltzmann simulation of viscoplastic fluids on natural convection in an inclined enclosure with inner cold circular/elliptical cylinders (Part I: One cylinder)," Int. J. Heat Mass Transfer **123**, 1138 (2018).
[84]G. R. Kefayati, "Double-diffusive natural convection and entropy generation of Bingham fluid in an inclined cavity," Int. J. Heat Mass Transfer **116**, 762 (2018).
[85]G. R. Kefayati, "Thermosolutal natural convection of viscoplastic fluids in an open porous cavity," Int. J. Heat Mass Transfer **138**, 401 (2019).
[86]G. R. Kefayati, "An immersed boundary-lattice Boltzmann method for thermal and thermo-solutal problems of Newtonian and non-Newtonian fluids," Phys. Fluids **32**, 073103 (2020).
[87]G. R. Kefayati, A. Tolooiyan, A. P. Bassom, and K. Vafai, "A mesoscopic model for thermal-solutal problems of power-law fluids through porous media," Phys. Fluids **33**, 033114 (2021).